chemosensors

MDPI

Review

Metal-Organic-Frameworks: Low Temperature Gas Sensing and Air Quality Monitoring

Xiaohu Chen [1], Reza Behboodian [2], Darren Bagnall [3], Mahdiar Taheri [4] and Noushin Nasiri [1,*]

1 NanoTech Laboratory, School of Engineering, Faculty of Science and Engineering, Macquarie University, Sydney, NSW 2109, Australia; jayden.chen@hdr.mq.edu.au
2 School of Engineering, Central Queensland University, Sydney Campus, Sydney NSW 2000, Australia; behboodianreza@gmail.com
3 School of Engineering, Faculty of Science and Engineering, Macquarie University, Sydney, NSW 2109, Australia; darren.bagnall@mq.edu.au
4 Research School of Engineering, The Australian National University, Canberra, ACT 2601, Australia; mahdiar.taheri@anu.edu.au
* Correspondence: noushin.nasiri@mq.edu.au

Abstract: As an emerging class of hybrid nanoporous materials, metal-organic frameworks (MOFs) have attracted significant attention as promising multifunctional building blocks for the development of highly sensitive and selective gas sensors due to their unique properties, such as large surface area, highly diversified structures, functionalizable sites and specific adsorption affinities. Here, we provide a review of recent advances in the design and fabrication of MOF nanomaterials for the low-temperature detection of different gases for air quality and environmental monitoring applications. The impact of key structural parameters including surface morphologies, metal nodes, organic linkers and functional groups on the sensing performance of state-of-the-art sensing technologies are discussed. This review is concluded by summarising achievements and current challenges, providing a future perspective for the development of the next generation of MOF-based nanostructured materials for low-temperature detection of gas molecules in real-world environments.

Keywords: metal-organic frameworks; hybrid nanomaterials; gas sensing; selectivity; sensitivity

Citation: Chen, X.; Behboodian, R.; Bagnall, D.; Taheri, M.; Nasiri, N. Metal-Organic-Frameworks: Low Temperature Gas Sensing and Air Quality Monitoring. *Chemosensors* **2021**, *9*, 316. https://doi.org/10.3390/chemosensors9110316

Academic Editors: Andrea Gaiardo, Barbara Fabbri and Vincenzo Guidi

Received: 5 October 2021
Accepted: 2 November 2021
Published: 8 November 2021

1. Introduction

In recent decades, the rapid growth of urban populations has resulted in new public health concerns and environmental pollution [1,2], and the fast monitoring of air- and water-borne contaminants using effective sensors has grown considerably in importance [1,3]. An effective sensor should interact with the target analyte selectively with high sensitivity and short response time [2,4–6]. In addition, the sensor should be cost-effective and demonstrate high reusability and reproducibility [2,7]. Sensors can be utilized to detect pollutants/analytes in aqueous (such as heavy metals, toxic organic compounds, and antibiotics) and gaseous form (such as volatile organic compounds, toxic gases, and greenhouse gases) [2,6,8,9]. The latter has a wide range of applications in food quality processes, industrial gases detection, and disease diagnosis, as well as indoor air-quality monitoring [8,10–12].

Several gas-sensing techniques have been developed including optical, capacitive, chemoresistive, and magnetic sensors [8,13–33]. In optical sensing, material optical properties change upon adsorption of the target analyte onto the surface producing an optical signal such as a change in visible colour, refractive index, luminescence intensity, etc. [27,32]. Capacitive-based sensors are an attractive class of sensors, in which capacitance changes due to the change in the dielectric permittivity upon adsorbing the gas/vapour molecules are detected [28–30]. In chemoresistive detectors, electrical conductivity changes as a result of a reaction between the target gas and oxygen molecules adsorbed on the surface

of the sensing material [4,21,33]. Generally, chemoresistive-based gas sensors provide a superior sensing response at room temperature compared to optical-based gas sensors. However, their slow response dynamic at low/room operating temperature and their lack of selectivity towards target gases hinder their real-world application [4–6].

In magnetic gas sensors, the magnetic properties of the sensing material are changed upon exposure to the target gas molecules; the change can be measured by, for example, application of the Hall effect, magnetization, spin orientation, ferromagnetic resonance, the magneto-optical Kerr effect, or the magnetostatic wave oscillation effect [8,13–15,17–26,31,34,35]. Sensing materials for gas detection can be classified into metal oxides [16,36,37], conductive and non-conductive polymers [38–41], carbon-based materials (e.g., graphene, carbon nanotubes, etc.) [42–46], noble metal-based structures [47–50], ionic liquids [51–53], metal-organic frameworks [8,54–56], and their composites [57–59]. Among these material groups, metal oxide-based sensors have been investigated extensively due to their strong and rapid response, low limit of detection (LOD), high reproducibility, simple and portable design, and low fabrication cost [60–62]. In recent years, the development of nanostructures and nanocomposites of metal oxide sensors has further improved device sensing characteristics. Despite these advantages and improvements, high operating temperature and inadequate gas selectivity have hindered substantial growth into new markets [61,63,64]. Polymers have been utilized in gas sensors as a sensing agent (mainly in a functionalized state) or immobilizing component to overcome some of these challenges [38,65]. Although significant progress in polymer sensors has been achieved over the last 20 years, these sensors encounter difficulties, including complex sensing mechanisms, poor selectivity towards target gases, a slow response dynamic, and significant matrix aging [22,38].

MOFs, a class of porous coordination polymers (PCPs), are crystalline frameworks with open porosity and are composed of metal nodes and organic linkers [66,67]. Over the last two decades, numerous compounds have been synthesised by changing the metal ions and organic ligands to produce materials with exceptional properties, including large surface area (surface areas more than 1,000 m^2g^{-1}), adjustable pore size, and tunable functional groups [8,21,68]. The manifold approaches for MOF synthesis, including the most versatile and widely used solvothermal methods, and recently realised green approaches, such as solvent-free mechanochemical routes [69–72], are making the process of preparing high-quality MOF-based materials easier and more environmentally friendly. Hence, MOFs have attracted much attention for numerous potential applications such as gas absorption/storage, gas separation, gas sensing, catalysis, solar energy conversion, energy storage, and biomedical technology/drug delivery [71,73–77].

Among the unique properties of MOFs, the reversible and selective adsorption of guest molecules onto their large surface areas is of great importance for sensing applications [2,54]. In fact, a high concentration of target gases inside a highly porous structure boosts the sensitivity of the sensor and the control over functional groups and pore sizes of the framework enhances the selectivity of the detection process [54]. Furthermore, in contrast to carbon-based and metal oxide-based sensors, which require high working temperature, MOF-based sensors have shown promising performances at low/room temperatures, resulting in significant reductions in power consumption, ease of manufacture and broadened application areas [78–81]. The variation in MOFs' physical and chemical properties following the adsorption of intended gas molecules has been exploited for the effective monitoring of environmental pollutants, indoor air quality, medical diagnosis and other areas of application [8,11,29,82,83].

Here, we present recent advances in the design and fabrication of MOF-based nanosensors for low concentration detection of different gases including nitrogen dioxide (NO_2), hydrogen sulfide (H_2S), sulfur dioxide (SO_2), carbon dioxide (CO_2) and ammonia (NH_3), for air quality and environmental monitoring applications. We critically assess and compare state-of-the-art MOF-based nanostructured technologies that are leading the way in developing sensitive and selective gas sensors with low operating temperatures

(Table 1). We focus on the impact of nanostructured morphologies, metal nodes, organic linkers, and functional groups, as well as gas-sensing mechanisms on the performance of state-of-the-art sensing technologies. We conclude with a review of the rapidly emerging trends and promising strategies that can enhance functionality and enable the production of the next generation of highly sensitive and selective MOF-based gas sensors for the low-temperature detection of gas molecules.

Table 1. Key features of MOF-based gas sensors for air quality monitoring.

Gas	Materials	Sensor Type	Working Cond.	Con./LOD (ppm)	Response ##	T_{res}/T_{rec} $$	Ref.
NO_2	Tb-MOF	Optical	RT, UV (350 nm)	5/1.8	0.55 (ΔPL/PL) *	<2 min [a]/~2 min	[84]
	Eu-MOF	Optical	RT, UV (350 nm)	5/2.2	0.11 (ΔPL/PL) *	90 s [b]/-	[84]
	MOF-A	Optical	RT	100%/-	Red to yellow during exposure	\	[85]
	MOF-A	Chemoresistive	RT, 0.5 V	100%/-	Resistance decreased from 0.57 TΩ to 0.25 MΩ then further down to 9.1 KΩ	2 min/42 s [c]	[85]
	Y-DOBDC	Optical	RT, UV/Vis	\	Yellow to brown–orange (@Vis illumination)	\	[32]
	Ni-MOF-74	Capacitive	50 °C, 10 mHz-1MHz	5/<0.5	725 (R_1/R_2) [d]	\	[86]
	In_2O_3/ZIF-8	Chemoresistive	140 °C	1/0.01	16.4 (R_g/R_a)	80 s/133 s	[87]
	$Cu_3(HHTP)_2/Fe_2O_3$	Chemoresistive	RT, Blue light	5/0.011	63.5% ($\Delta R/R_0$)	\	[88]
	Pd@$Cu_3(HHTP)_2$	Chemoresistive	RT, 5%RH	5/-	−62.11% ($\Delta R/R_0$)	13.8 min/-	[89]
	Pt@$Cu_3(HHTP)_2$	Chemoresistive	RT, 5%RH	5/-	−57.38% ($\Delta R/R_0$)	14 min/-	[89]
	Pt@$Cu_3(HHTP)_2$	Chemoresistive	RT	3/0.1	89.9% ($\Delta R/R_0$)	8.2 min/-	[90]
	$Cu_3(HHTP)_2$	Chemoresistive	RT	3/0.1	53.7% ($\Delta R/R_0$)	14 min/-	[90]
	ZIF-8-8 [1]	Chemoresistive	350 °C, 5 V	100/-	~118.5 (R_g/R_a)	113.5 s/111.5 s	[91]
H_2S	MIL-100(In) [2]	Optical	40 °C	3/0.535	2200 (PL) *	\	[92]
	fum-fcu-MOF	Capacitive	RT	1/0.0054	8.8×10^{-4} (Δc/c)	\	[93]
	ZIF-8/ZnO	Chemoresistive	RT	1/≤0.05	18.7% ($\Delta R/R_0$)	7 min/10.7 min	[94]
	MOF-5/CS/IL [3]	Chemoresistive	RT, 120 mV	100/1	98% (R_a/R_g)	<8 s/~30 s	[95]
	$Cu_3(HHTP)_2$	Chemoresistive	RT	80/0.52	98% ($-\Delta G/G_0$)	5 min/10 min [e]	[96]
	$Ni_3(HHTP)_2$	Chemoresistive	RT	80/0.23	97% ($-\Delta G/G_0$)	5 min/10 min [e]	[96]
	NiPc-Ni [4]	Chemoresistive	RT, 0.01–1.0 V	80/0.032	64% ($-\Delta G/G_0$)	2.3 min/10 min [e]	[97]
	NiPc-Cu [4]	Chemoresistive	RT, 0.01–1.0 V	80/0.019	98% ($-\Delta G/G_0$)	1.3 min/10 min [e]	[97]

Table 1. *Cont.*

Gas	Materials	Sensor Type	Working Cond.	Con./LOD (ppm)	Response [##]	T_{res}/T_{rec} [$$]	Ref.
SO_2	MOF-5-NH_2	Optical	RT, UV (365 nm)	2/0.05	Luminescence turn-on	15 s/-	[98]
	Eu-BDC-NH_2 [5]	Optical	RT, UV (370 nm)	10/0.65	7340 (PL) *	6 s/-	[99]
	UiO-66-NH_2	Capacitive	RT	50/-	23×10^{-4} ($\Delta c/c$)	185 s/-	[28]
	MFM-300(In)	Capacitive	RT (22 °C)	1/0.005	17×10^{-4} ($\Delta c/c$) *	\	[100]
	NH_2-UiO-66	Chemoresistive	150 °C	10/1	21.6% ($\Delta R/R_0$)	26.8 s/41.6 s	[101]
	Ni-MOF/–OH-SWNTs	Chemoresistive	RT	1/0.5	0.9784 ($\Delta R/R_0$)	10 s/30 s	[102]
CO_2	ZIF-8	Optical	RT, UV (242 nm)	60%/-	72% (T%) *,[f]	14 s/9 s	[103]
	Mg-MOF-74	Capacitive	RT	1000/-	2.1×10^{-4} ($\Delta c/c$) *	\	[9]
	NH_2-UiO-66(Zr)	Chemoresistive	150 °C,	5000/-	11.4% ($\Delta R/R_0$)	\	[101]
	Cu_3(HIB)$_2$	Chemoresistive	RT	400–2500/67	0.62% ($\Delta G/G_0$)	7–8 min/10–11 min	[104]
	SnO_2@ZIF-67	Chemoresistive	205 °C	5000/-	16.5% ($\Delta R/R_0$)	96 s/25 s	[105]
NH_3	MIL-124@Eu^{3+}/Al_2O_3	Optical	RT, UV (298 nm)	500/26.2	0.14 ($\Delta PL/PL$) *	\	[106]
	NDC-Y-fcu-MOF [6]	Capacitive	RT	25/0.092	7×10^{-4} ($\Delta c/c$) *	~250 s/	[107]
	NiPc-M [7]	Chemoresistive	RT, 0.01–1.0 V	80/0.05	43–45% ($-\Delta G/G_0$)	2.3–1.3 min/-	[97]
	Cu-BHT [8]	Chemoresistive	RT, 0.01 V	20/0.23	7.88% ($\Delta R/R_0$)	58 s/102 s	[108]
	Cu_3(HITP)$_2$	Chemoresistive	RT, 0.1 V	2/-	0.48% ($\Delta G/G_0$)	\	[109]
	Cu-HHTP	Chemoresistive	RT	100/8.7×10^{-5}	161% (R_a/R_g)	35 s/15 min	[110]
	Pd-Co@IRMOF1 [9]	Chemoresistive	RT	90/1	80.17 (R_a/R_g)	46 s/22 s	[111]
	Zn (NA) [10]	Chemoresistive	RT	100/-	220 (R_a/R_g)	46 s/200 s	[112]
	SNNU-88 [11]	Chemoresistive	RT	50/-	2.3 (R_a/R_g)	87 s/127 s	[113]
	Cu_3(BTC)$_2$/GO [12]	Chemoresistive	RT, 1 V	100/-	4 (R_a/R_g)	\	[114]

[##] In the Response column: "Δ" represents difference; PL, R, G and c correspond to intensity of photoluminescence emission, electric resistance, current, and capacitance, respectively; subscripts of "0", "a" and "g" refer to the initial state, in air and in target gas, respectively. [$$] T_{res} and T_{rec} are the sensor response and recovery time, respectively. * Estimated value, data is unavailable. [a] Time for emission peak (543 nm) to reach its plateau. [b] Time for ~20% increase in PL after exposure to target gas. [c] 2 min is for current increased from 30 nA to 2 μA, and 42 s is for current decreased from 55 μA to 30 nA. [d] R_1 and R_2 correspond to the resistance of M-MOF-74 before and after exposure to target gas. [e] Time for purging the target gas (H_2S) and dry N_2 respectively. [f] %T = transmittance. [1] The ZIF-8 was synthesised at a molar ratio of 8:1 for $Zn(NO_3)_2 \cdot 6H_2O$ and 2-methylimidazole. [2] MIL-100(In) = $In_3O(OH)(H_2O)_2[BTC]_2$, where indium is the metal node and BTC (1,3,5-benzenetricarboxylic acid) is the ligand. [3] MOF-5 ($[Zn_4O(BDC)_3]_n$) microplates embedded on an organic membrane of chitosan (CS) blended with glycerol ionic liquid (IL). [4] NiPc = nickel phthalocyanine. [5] Eu-BDC-NH_2 (H_2BDC-NH_2, 2-aminoterephthalic acid), where BDC = 1,4-benzodicarboxylate. [6] NDC-Y-fcu-MOF = Naphthalene (NDC) based RE-fcu-MOF, fcu is short for face-centred cubic. [7] M = Ni, Cu. [8] BHT= benzenehexathiol. [9] IRMOF-1 (MOF-5) is a metal-organic framework compound with the formula of $Zn_4O(BDC)_3$. [10] NA = nicotinic Acid. [11] SNNU-88= $\{[(CH_3)_2NH_2][Mg_3(OH)(DHBDC)_3(TPP)]\}_n$; where SNNU = Shaanxi Normal University, and TPP = 2,4,6-tri(4-pyridyl)pyridine. [12] BTC = benzene tricarboxylic, GO = graphene oxide.

2. Nitrogen Dioxide (NO_2)

Among the most common pollutants, NO_2 is a harmful gas that is generated by combustion processes at high temperatures and requires to be monitored in order to control its release [115]. NO_2 is the main source of nitric acid aerosol leading to smog and acid rain; in humans, it can cause inflammation of the airways and can even cause death at high concentrations [116,117]. Therefore, there is great demand for highly sensitive, selective, cost-effective, rapid and reliable, non-invasive techniques for monitoring NO_2.

Monitoring the optical emission changes of the MOF pre- and post-NO_2 exposure provides an interesting route for the utilization of MOF-based materials in gas-sensing

applications. Luminescent MOFs (LMOFs) are widely used in gas sensing because of their excellent optical response towards guest molecules inside their cavities. Gas sensors, fabricated using two lanthanide-based MOFs (Tb-MOF and Eu-MOF, formed by 2-amino-1,4-benzene dicarboxylic acid with europium and terbium salts, respectively), were reported by Gamonal et al. [84] for NO_2 gas detection with an LOD of 2.2 ppm at room temperature. The sensing mechanism was based on the rise in Eu^{3+} luminosity and the reduction in Tb^{3+} luminescence upon exposure to NO_2 gas. Zhang et al. [118] demonstrated a direct correlation between the fluorescence intensity of the ZJU-66-based sensor and NO_2 concentrations. Similarly, Moscoso et al. [119] developed Tb-based MOF films, so-called Tb(BTC)@PDMS (BTC: benzene-1,3,5tricarboxylate, PDMS: polydimethylsiloxane), where the photoluminescent frequency of the film was gradually decreased as the NO_2 concentration was increased from 0 to 500 ppm.

A combination of colorimetric and chemoresistive MOF detectors (MOF A, with Co and octadentate calix[4]-resorcinarene as the metallic centre and ligand, respectively) was synthesised by Ma et al. [90] using a solvothermal approach. The sensing mechanism was based on the absorption of NO_2 gas molecules onto the surface of MOF A. The O atoms of the absorbed NO_2 interacted primarily with the adjacent carboxylic groups and coordinating water through hydrogen-bonding interactions, leading to the formation of a conductive pathway. Another conductive pathway may be formed by the NO_2 molecule and H_3O^+ through hydrogen-bonding interactions (Figure 1b, inset), resulting in an eight orders of magnitude enhancement for conductivity where the resistance of MOF A decreased from 5.7×10^{11} Ω to 9.1×10^3 Ω upon exposure to NO_2 gas molecules (Figure 1b). In addition to the electrical sensing response, a visible change in the colour was observed in MOF A where the crystal colour changed from red to yellow after NO_2 exposure (Figure 1a).

In a similar gas molecule absorption approach, Gallis et al. [32] reported the NO_x adsorption behaviour of Y-DOBDC-based MOF (yttrium-2,5-dihydroxyter-ephthalic acid) by analysing its photoluminescence (PL) characteristics in both pre-NO_x and post-NO_x exposures. As demonstrated in Figure 1c, the colour of synthesised Y-DOBDC-based MOF changed from pale yellow to vibrant brown–orange after NOx exposure for 24 h under visible light. In addition, a significant reduction in the emission intensity of all compounds was observed under UV light illumination (350 nm) after 24 h exposure (Figure 1d), indicating the interaction between the DOBDC ligand in Y-DOBDC and NO_2 molecules (Figure 1d, inset). Observed and detectable optical signals upon the absorption of NO_2 gas provided a unique and direct means for NO_2 detection; however, quantitative analysis of the variable of NO_2 concentration was not addressed in detail [85].

Liu et al. [87] reported an In_2O_3/ZIF-8 (ZIF-8: zeolitic imidazolate framework-8, where Zn and 2-methylimidazole are the metal node and ligand, respectively) nanocomplex for ppb-level NO_2 gas detection, with enhanced humidity resistance due to the hydrophobic nature of the self-templated ZIF-8 nanoparticles on the surface of In_2O_3 nanofibers. The synthesis procedure involved electrospinning and subsequent calcination in the air to fabricate In_2O_3/ZnO, which was not only used as the Zn^{2+} source for subsequent ZIF-8 solvothermal growth on the surface of In_2O_3 nanofibers (Figure 2a,b) but also as the template for the In_2O_3/ZIF-8 nanocomplex. Different microstructures of the In_2O_3/ZIF-8 nanohybrid were prepared by tuning the molar ratios of In and Zn from 8:1 to 2:1 (Figure 2c–e) where ZIF-8 NPs (80–100 nm in diameter) were attached to the surface of the In_2O_3 nanofibers.

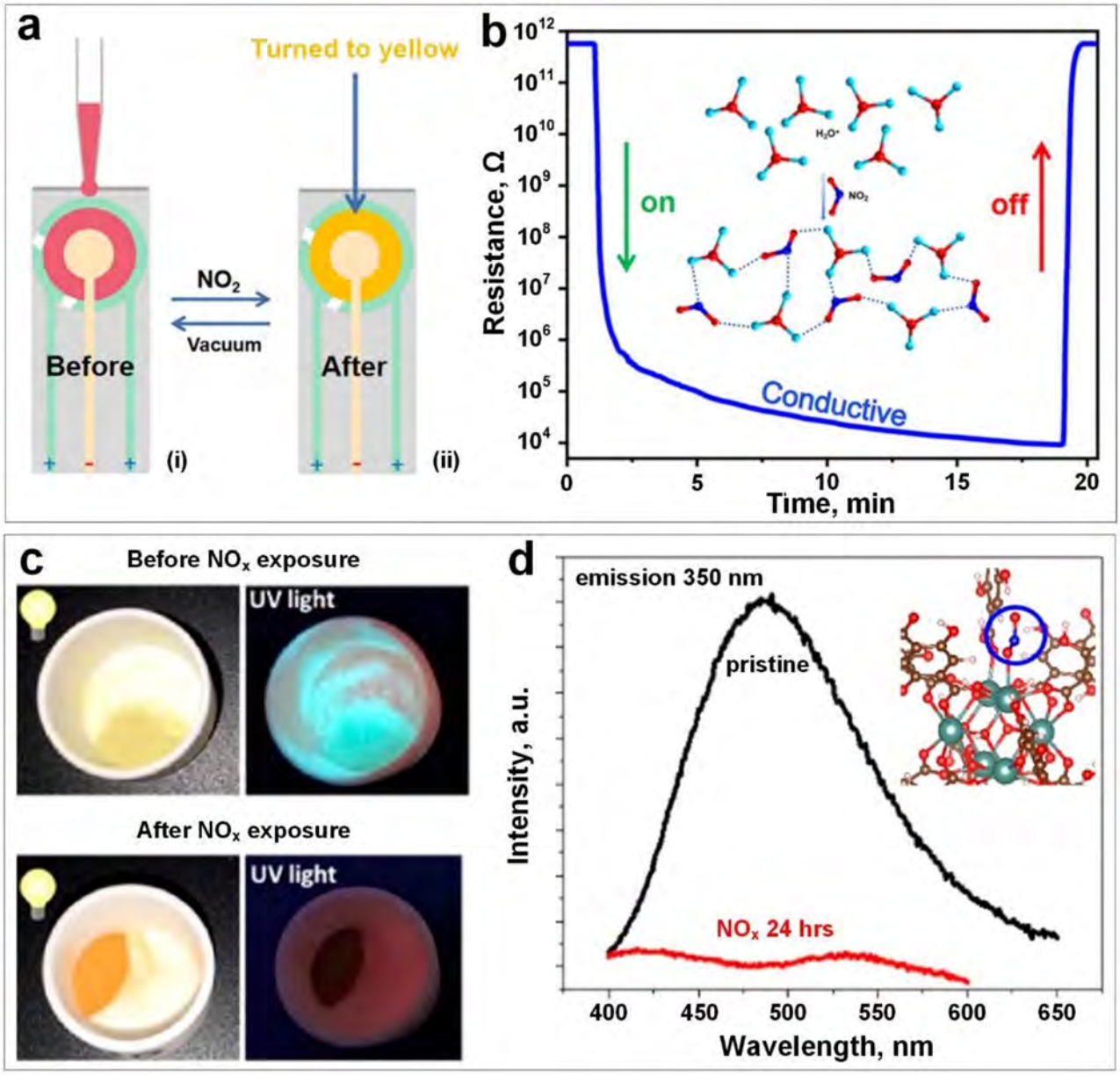

Figure 1. (**a**) The colour change in a gold electrode sheet covered by MOF A before and after NO_2 exposure. (**b**) The resistance variation versus time upon NO_2 exposure. Reproduced with permission from [85] American Chemical Society, 2021. (**c**) The colour change of Y-DOBDC before and after exposure to NO_x under visible and UV light. (**d**) Photoluminescent intensity of Y-DOBDC before and after 24 h exposure to NO_x, and the guest-framework interactions (Inset). Reproduced with permission from [32] American Chemical Society, 2019.

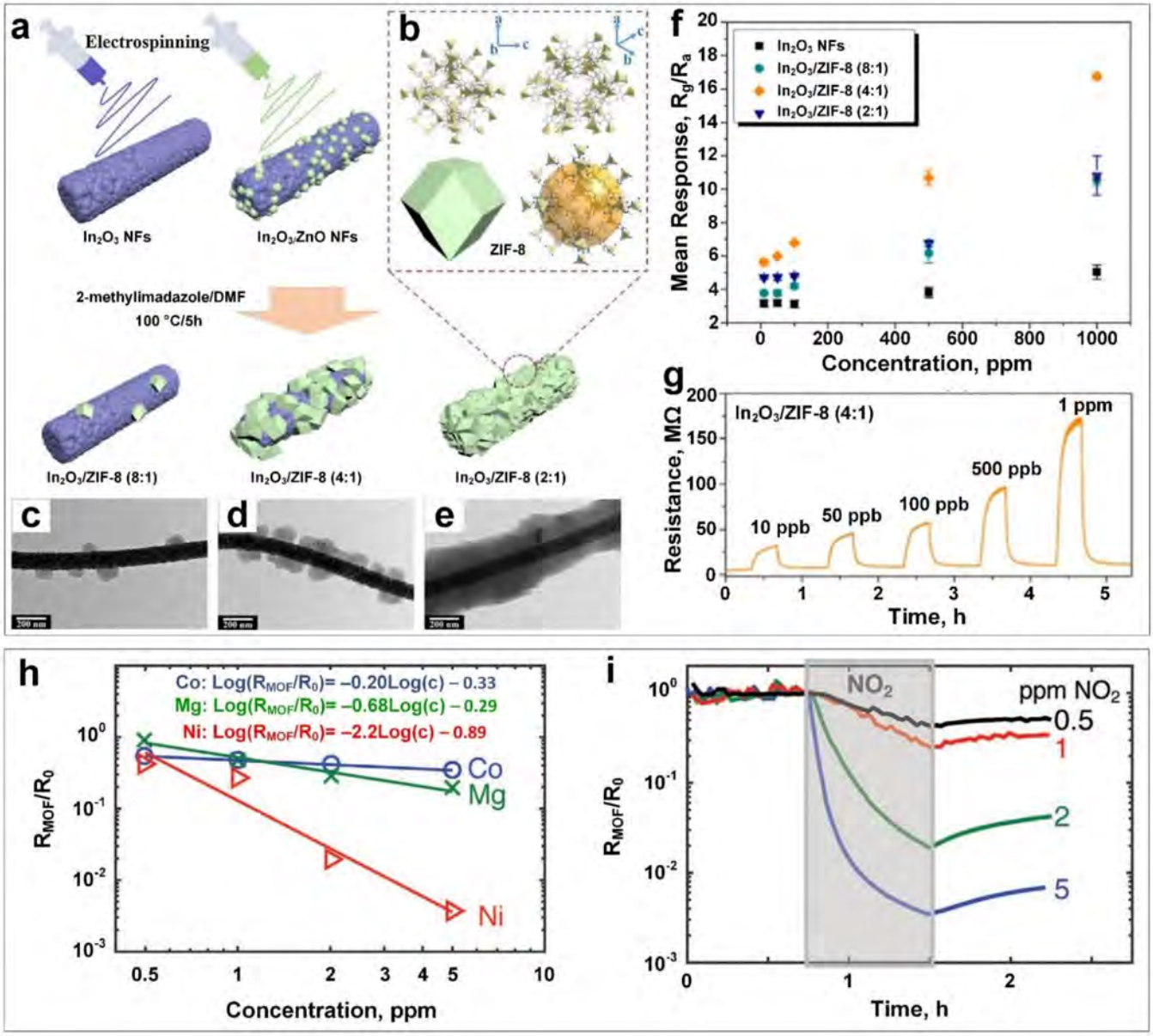

Figure 2. (**a**) Schematic diagram of In_2O_3/ZIF-8 nanocomposite fabrication. (**b**) ZIF-8 structure. TEM images of In_2O_3/ZIF-8 (8:1) (**c**), In_2O_3/ZIF-8 (4:1) (**d**), and In_2O_3/ZIF-8 (2:1) (**e**). (**f**) Mean response versus concentration for pure In_2O_3 and its composites with ZIF-8. (**g**) Typical dynamic response curves of In_2O_3/ZIF-8 (4:1) sensors towards NO_2 gas at different concentrations at 140 °C. Reproduced with permission from [87] Elsevier, 2019. (**h**) The relationship of response versus NO_2 gas concentration for different M−MOF−74 (M = Co, Mg, Ni). (**i**) The dynamic response curves of M−MOF−74 for exposure to 0.5, 1, 2 and 5 ppm NO_2 gas at 50 °C. Reproduced with permission from [86] Wiley-VCH, 2020.

The fabricated In_2O_3/ZIF-8 with a molar ratio of 4:1 (In: Zn) demonstrated the highest sensing response among all the In_2O_3/ZIF-8 nanocomposites (and pure In_2O_3) within the NO_2 concentration range of 10 ppb to 1 ppm at an optimal operating temperature of 140 °C (Figure 2f). A sensing response of 16.4 was achieved for In_2O_3/ZIF-8 (4:1) at 1 ppm NO_2 concentration compared to 10.7, 10.4 and 4.9 for In_2O_3/ZIF-8 (2:1), In_2O_3/ZIF-8 (8:1) and In_2O_3 respectively. For a typical dynamic NO_2 gas-sensing curve based on In_2O_3/ZIF-8 (4:1) (Figure 2g), a well-defined increasing resistance trend was reported with increasing NO_2 gas concentration. In addition, rapid response kinetics of 80 s and 133 s for response and recovery time, respectively, were achieved for the In_2O_3/ZIF-8 (4:1)

nanosensor, demonstrating that In_2O_3/ZIF-8 (4:1) is a promising nanostructured candidate for the fast detection of NO_2 gas down to 10 ppb at an operating temperature of 140 °C.

Using a different approach, a macroscale (~35 mm^2) capacitive M-MOF-74-based sensor (formed by divalent metallic cations with the organic ligand of 2,5- dihydroxyterephthalic acid) was designed by Small et al. [86] via a solvothermal synthesis technique for NO_2 gas sensing at 50 °C with a near-zero power consumption of 2.25 pW. The sensing performance of the fabricated device towards NO_2 gas concentrations of 0.5 to 5 ppm was investigated as a function of metal centres in the synthesised MOF-74 (i.e., Ni, Co, Mg). As illustrated in Figure 2h, the Ni-based sensor (Ni-MOF-74) demonstrated the largest change in the film resistance and consequently a higher sensing response towards NO_2 gas at different concentrations. However, the fabricated device suffered from very slow response dynamics and irreversible sensing performances (Figure 2i), hindering its real-world application. The former could be attributed to its high resistance change (orders of magnitude) upon NO_2 exposure and the significantly large crystallite size of Ni-MOF-74 (up to 100's of μm), making the difference in mass transport of NO_2 less dominant at short time intervals. The issue of prolonged recovery time towards NO_2 gas sensing might be addressed by using a photoactivation approach [88].

Catalytic metal nanoparticles (NPs, e.g., Au, Pd and Pt) have long been proved to boost the gas-sensing performance chemoresistively [120–122]. Taking advantage of self-assembled highly porous 2D conductive MOFs with tuneable cavity size, Koo et al. [89] introduced well-dispersed Pd and Pt NPs to solvothermally fabricated Cu_3(hexahydroxytriphenylene)$_2$ ($Cu_3(HHTP)_2$) with 2 nm cavities (Figure 3a). Upon exposure to 5 ppm NO_2, both $Cu_3(HHTP)_2$ and M@$Cu_3(HHTP)_2$ (M = Pd, Pt) exhibited p-type semiconducting characteristics, with a significantly higher sensing response (about two times higher) for both Pd@$Cu_3(HHTP)_2$ and Pt@$Cu_3(HHTP)_2$ (62.11% and 57.38%, respectively) compared to the pure $Cu_3(HHTP)_2$ (response of 29.95%) (Figure 3c). This higher sensing performance could be attributed to the electronic sensitization mechanism resulting from the lowering of potential barriers at Schottky junctions between metallic NPs and $Cu_3(HHTP)_2$ as NO_2 molecules were absorbed on the surface (Figure 3b). The reduced sensing performance of the Pt-based sensing material could be attributed to the higher NO_2 adsorption and desorption kinetics of Pt-decorated MOF (5.54×10^{-2} $ppm^{-1} \cdot s^{-1}$ and 7.30×10^{-5} $ppm^{-1} \cdot s^{-1}$ for adsorption and desorption, respectively) compared to those of Pd-decorated MOF (2.51×10^{-2} $ppm^{-1} \cdot s^{-1}$ and 5.10×10^{-5} $ppm^{-1} \cdot s^{-1}$ for adsorption and desorption, respectively).

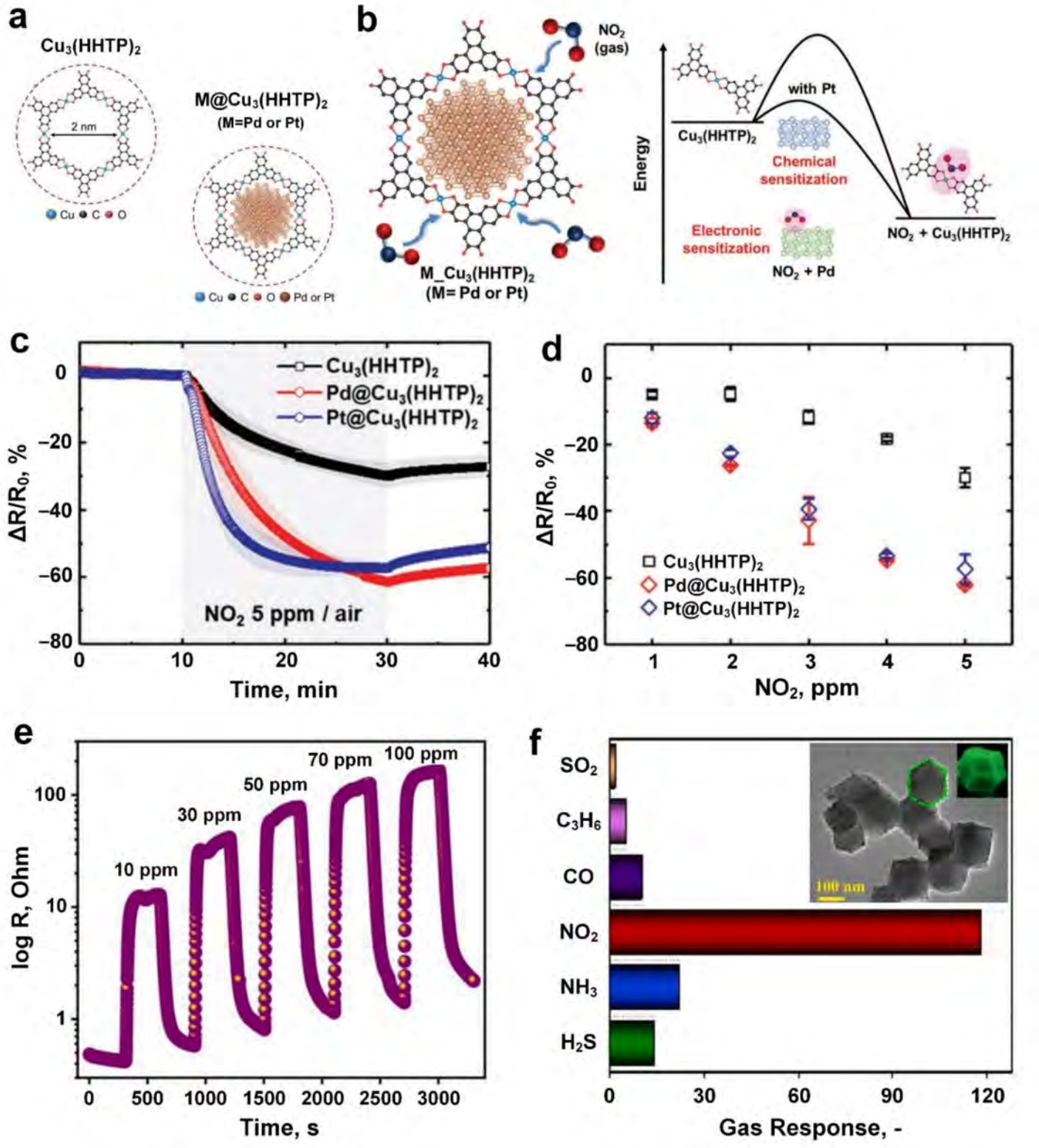

Figure 3. (**a**) Schematic of $Cu_3(HHTP)_2$ and $M@Cu_3(HHTP)_2$ structures, and (**b**) the sensing mechanism towards NO_2 gas. (**c**) The response dynamics of $Cu_3(HHTP)_2$ and $M@Cu_3(HHTP)_2$ (M = Pd, Pt) sensors to 5 ppm NO_2 gas, and (**d**) the corresponding responses for a range of NO_2 concentrations. All tests were performed at room temperature in the air. Reproduced with permission from [89] Wiley, 2019. (**e**) The dynamic response of ZIF−8−8 sensor versus different concentrations of NO_2 gas at 350 °C. (**f**) The cross-selectivity of ZIF−8−8 sensors towards 100 ppm of different gases at 350 °C (Inset, TEM image of nanostructured polyhedral ZIF−8−8). Reproduced with permission from [91] Elsevier, 2021.

The sensing response increased linearly from ~6% to ~60% with an increase in NO_2 concentration from 1 ppm to 5 ppm (Figure 3d) indicating that M@Cu_3(HHTP)$_2$ (M = Pd, Pt) is a promising candidate for room temperature NO_2 sensing applications. In addition to the higher sensing response, a faster response kinetic was reported for Pd@Cu_3(HHTP)$_2$ and Pt@Cu_3(HHTP)$_2$ with 13.8 min and 14 min response time, respectively, while a significantly longer response time of >18 min was observed for the non-NP decorated Cu_3(HHTP)$_2$.

Recently, a novel microfluidic channel-embedded solution-shearing (MiCS) fabrication scheme was proposed for the large-area synthesis of MOF-based thin films (tens of nanometres) for the room temperature detection of NO_2 gas molecules [90]. Here, similar to the blade-coating technique, a solution-to-solid transition close to the edge of the meniscus was formed between a moving blade and a heated substrate resulted in the deposition of a thin film on the substrate [123]. Applying this innovative method, Pt@Cu_3(HHTP)$_2$ with optimized (2.3 wt.%) Pt-loading demonstrated a superior gas sensing performance towards NO_2 molecules with a high response of 89.8% and a short response time of 8.2 min. Compared to Pt@Cu_3(HHTP)$_2$ fabricated previously via the conventional solvothermal method [89], the synergetic effects of large surface area and high porosity of the ultrathin MOF structure, as well as embedded nanoscopic Pt catalysts, are the major factors affecting enhanced NO_2 gas sensing performance.

In another approach, ZIF-8 nanoparticles (Figure 3f, inset) were fabricated via a solvothermal method for NO_2 gas sensing applications [91]. Different ratios of $Zn(NO_3)_2.6H_2O$ to 2-methylimidazole from 8:1 to 64:1 were used in the synthesis of the ZIF-8 (they were named accordingly as ZIF-8-8, ZIF-8-16, ZIF-8-32 and ZIF-8-64). The fabricated ZIF-8-8 demonstrated the highest sensing response of ~118.5 (R_g/R_a, where R_g and R_a are the resistance of ZIF-8-8 in the target gas and air, respectively) at 100 ppm NO_2 concentration (Figure 3e), which was four-times that of other ZIF-8 based gas sensors. This higher sensing performance for ZIF-8-8 could be attributed to the larger specific surface area of ZIF-8-8 compared to ZIF-8-16, ZIF-8-32 and ZIF-8-64 nanoparticles.

In addition to high sensitivity, the fabricated ZIF-8-8 also demonstrated outstanding selectivity towards NO_2 gas among a variety of gases (Figure 3f). This excellent selectivity could be attributed to the relatively low bond energy of NO_2 (466 KJ·mol^{-1}) compared to the comparatively high bond energy of other gaes (such as the bond energy of 1072 KJ·mol^{-1} for CO molecules) [91]. Moreover, the sensitivity of the synthesized ZIF-8 nanomaterials was investigated over time, demonstrating an excellent stability/repeatability for the ZIF-8-8 nanosensor (compared with the other three ZIF-8 based samples) with only a 36.6% reduction in sensing response (from 112 to 71) after 54 days. Novel strategies such as to form hybrid nanocomposites with metal oxides (e.g., In_2O_3 [87]) could open new avenues to reduce the working temperature of current state-of-the-art technologies.

3. Hydrogen Sulphide (H_2S)

H_2S is another air pollutant gas formed in large quantities by a range of activities, including some common large-scale activities such as sewerage processing and oil refining. In humans, H_2S can cause significant health concerns including allergic reactions and lung inflammation [124]. Despite significant advances in the design of highly sensitive H_2S gas sensors, continuous monitoring of trace-level (sub-ppm) H_2S at low operating temperatures is still challenging [125]. Given that H_2S is such a significant contaminant and is generated in several industrial applications, developing real-time sensitive and selective gas-sensing technologies for rapid detection of this gas is critical.

Zhang et al. [92] reported, for the first time, the fluorescence sensing of H_2S gas molecules through the post functionalisation of MIL-100(In) films with metal ions including Eu^{3+} and Cu^{2+} (Figure 4a,b). The sensing mechanism in this device was based on the reaction between Cu^{2+} ions and H_2S gas molecules, resulting in the activation of Eu^{3+} emission (Figure 4c). The fluorescence response of the MIL-100(In)@Eu^{3+}/Cu^{2+} film with a range of H_2S concentrations at an operating temperature of 40 °C is presented in Figure 4d,e. The fluorescence intensity of MIL-100(In)@Eu^{3+}/Cu^{2+} was found to increase

steadily with the increase in H_2S level from 0 to 115 ppm (Figure 4d), with a linear increase in the luminescence intensity as a function of H_2S level (Figure 4e), and a detection limit of 0.535 ppm.

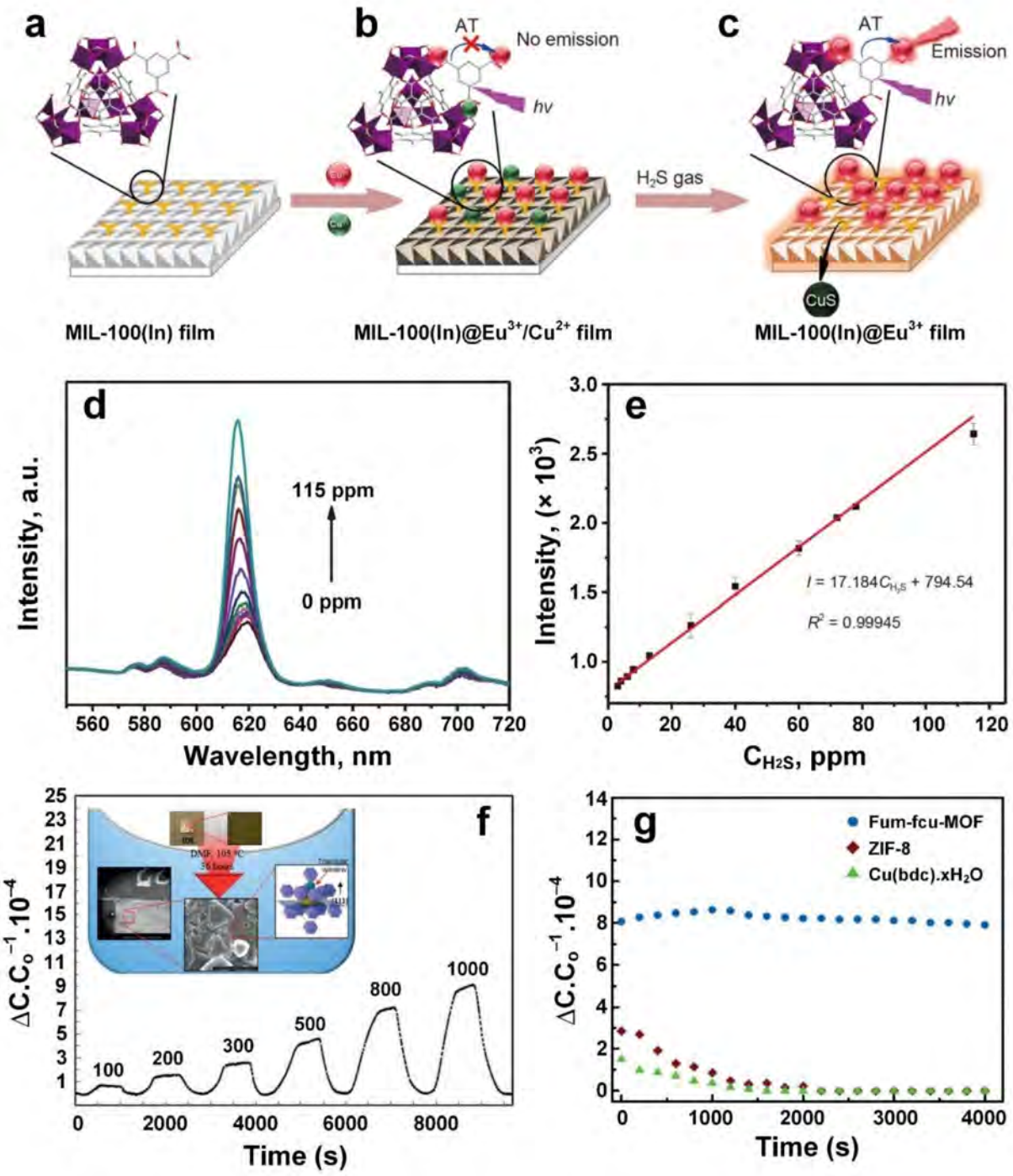

Figure 4. Schematic illustrations of MIL-100(In) based fluorescence sensor for H_2S gas detection: The MIL-100(In) film coordinating BTC ligands on the surface (**a**) can be functionalized by Eu^{3+}/Cu^{2+} ions simultaneously with no emission of Eu^{3+} (**b**); however, the characteristic emission of Eu^{3+} in MIL-100(In)@Eu^{3+}/Cu^{2+} film could turn on with the presence of H_2S gas (**c**). (**d**,**e**) Fluorescence intensity versus H_2S gas at different concentrations at 40 °C. Reproduced with permission from [92] Springer, 2019. (**f**) The dynamic response curves of fum−fcu−MOF against H_2S gas at different concentrations, and the microstructure of fum−fcu−MOF coated on IDE (Inset). (**g**) The stability performance of fum-fcu-MOF against ZIF-8 and Cu(BDC)·xH_2O MOF. Reproduced with permission from [93] Wiley-VCH, 2016.

Using a solvothermal technique and an in situ crystallisation method, Yassine et al. [93] reported the development of an isoreticular rare-earth-metal-based MOF on the surface of capacitive interdigitated electrodes (IDEs). This resulted in homogenous growth of highly oriented small crystals of fumarate-based fcu-MOF (fum-fcu-MOF, fcu is short for face-centred cubic) thin film with remarkable sensitivity towards low concentration of H_2S at room temperature (Figure 4f, inset). The IDEs were pre-functionalized with an OH-terminated monolayer (11-mercaptoundecanol) prior to the growth of fum-fcu-MOF. The sensing performance of the fabricated crystals towards different gases was investigated after activation of the sample under vacuum for one hour. The device showed remarkable sensitivity towards H_2S at concentrations down to 100 ppb, with a linear sensing response and an impressive LOD of 5 ppb (Figure 4f).

In addition to high sensitivity, the sensor demonstrated excellent selectivity towards H_2S with almost negligible signals upon exposure to other gases, including CH_4, H_2 and C_7H_8 (toluene). A slight cross-sensitivity was detected towards NO_2 gas molecules; however, the sensing layer showed a six-fold higher sensing response to H_2S compared to NO_2 gas. This outstanding sensing performance could be attributed to the interconnected octahedral and tetrahedral cages of fum-fcu-MOF which significantly reduces the gas diffusion resistance and consequently enhances the sensing response to target gas.

The stability of sensing performance for the fum-fcu-MOF layer towards H_2S was investigated over a period of three months, exhibiting excellent stability and uniform detection levels over a range of cycles. To demonstrate the excellent stability of the fabricated sensor, the sensing performance of two other MOF sensors, namely, ZIF-8 and Cu(BDC)·xH_2O (BDC: benzenedicarboxylate), was tested for 4000 s. These tests revealed a significant reduction in the sensing performance of these devices after only 1000 s (Figure 4g). This lower stability could be attributed to the degradation of the MOF structures and the formation of metal sulphide components upon prolonged H_2S exposure. In contrast, the metal clusters in the fum-fcu-MOF structure were bridged by shorter and rigid liners, prohibiting the formation of metal sulphides.

A similar device concept was applied by Wu et al. [94], where the surface of a ZnO-based sensor was partially covered by porous ZIF-8 particles to improve the sensitivity and selectivity of sensing material towards H_2S gas molecules by providing larger surface areas (thus more active sites) and more abundant oxygen vacancies. This led to the expansion of the electron depletion region in the ambient atmosphere (Figure 5a) and resulted in better H_2S absorption and higher sensitivity upon gas exposure (Figure 5b). Since the pore dimension of ZIF-8 (3.4 Å) is slightly smaller than the diameter of H_2S gas (3.6 Å), the adsorbed H_2S gas molecules via active sites on the surface of ZIF-8 particles were pre-concentrated before transferring and being exposed to the ZnO surface. This partial coverage of ZnO by ZIF-8 was preferable over fully covered ZnO, as H_2S gas molecules could reach the surface of ZnO nanorods with no diffusion limitation through ZIF-8 particles.

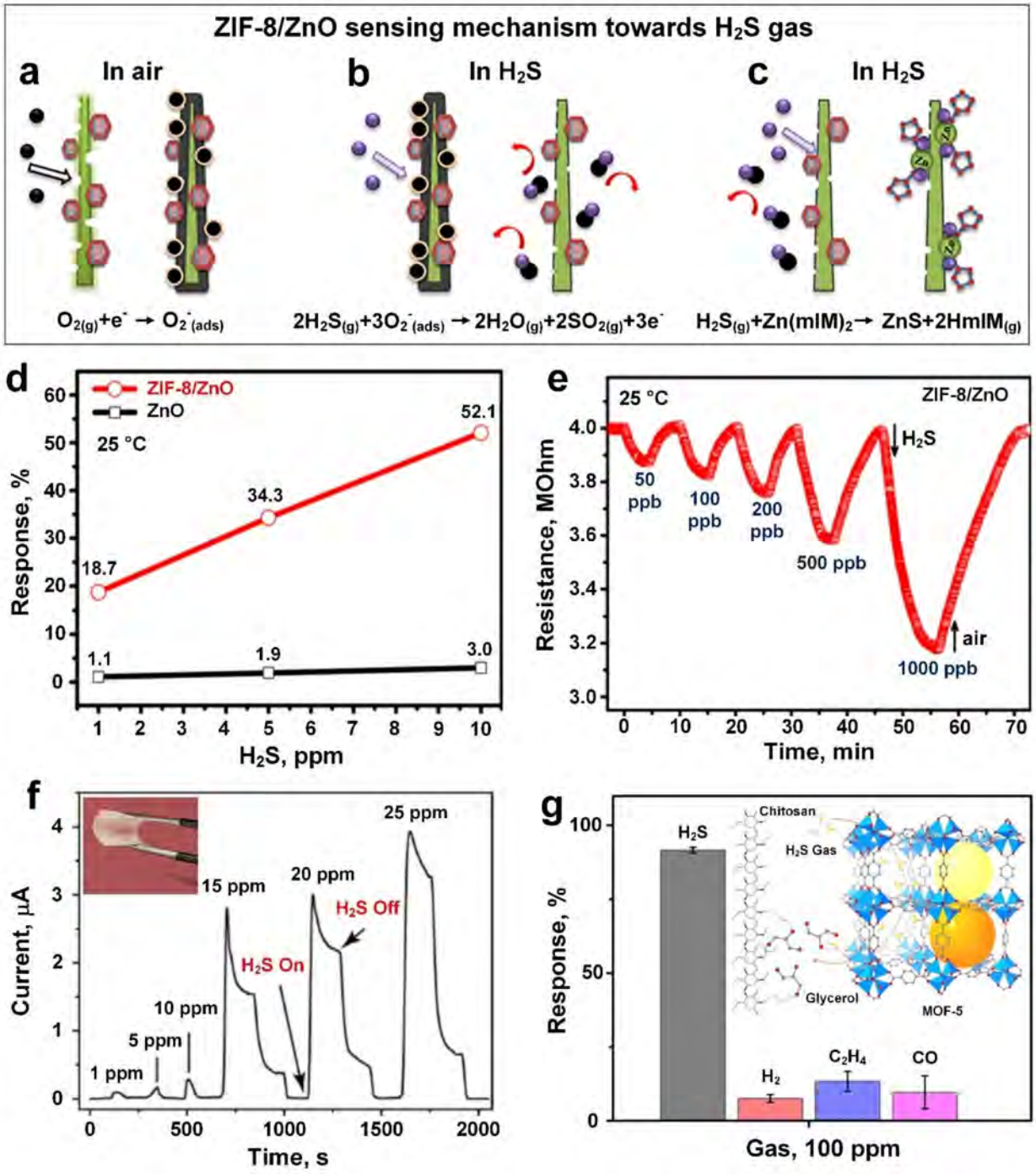

Figure 5. Schematic representation of ZIF-8/ZnO sensing mechanism towards H_2S gas: (**a**) the surface depletion region was expanded due to more electrons were trapped by the surface chemisorbed oxygen before the sensor was explosed to H_2S gas, the sensor exhibited a high base resistivity consequently; (**b**) when sensor was exposed to H_2S gas, the chemisorbed oxygen would react with H_2S molecules chemically to release the trapped electons, resulting in the reduction of depletion region and significant causing resistivity change; (**c**) H_2S gas might interact with Zn $(mLm)_2$ transformed from ZIF-8 to form an intermediate product (ZnS) to further enhance the sensitivity towards H_2S gas. (**d**) The response of ZnO and ZIF-8/ZnO toward 1, 5 and 10 ppm of H_2S gas at 25 °C. (**e**) The dynamic resistance curves of ZIF-8/ZnO against H_2S gas at ppb-level concentration. Reproduced with permission from [94] Elsevier, 2019. (**f**) The electrical current variation of MOF-5/CS/IL membrane against H_2S gas at different concentrations, and the flexibility demonstration of MOF-5/CS/IL membrane as inset. (**g**) The high cross-selectivity of MOF-5/CS/IL membrane towards H_2S compared with H_2, C_2H_4 and CO gases, and the possible sensing mechanism for the outstanding H_2S gas response. Reproduced with permission from [95] American Chemical Society, 2021.

In addition, the reaction between ZIF-8 nanoparticles and H_2S gas results in the formation of ZnS (Figure 5c), which reduces the depletion region even further and plays a key role in the high selectivity of the developed sensing material towards H_2S over other reducing gases.

The sensing performance of the fabricated ZIF-8/ZnO device is presented in Figure 5d, demonstrating a sensing response of 18.7% and 52.1% towards H_2S gas with concentrations of 1 and 10 ppm, respectively (Figure 5d, red circles), which is correspondingly 18 and 15 times higher than for the pure ZnO nanorods (Figure 5d black rectangles). The well-performed ppb-level H_2S gas-sensing capability is presented in Figure 5e, starting at a very low concentration of 50 ppb. The resistance changed steadily with increasing H_2S concentration up to 1 ppm.

Despite the hydrophobic and moisture-resistive properties of ZIF-8 (demonstrating a contact angle of $138 \pm 1.5°$), the sensor was still vulnerable in a humidity environment with RH over 50%, showing an adverse impact of the moisture on the performance of H_2S gas sensing. In addition, a slow response dynamic with a long response time of 7 min was recorded upon exposure to 1 ppm of H_2S gas. Further modifications are required to improve the ZIF-8 stability in a high humidity environment for achieving further humidity-independent features and enhanced response dynamics [126].

By taking advantage of the cage-bridge structure of MOF-5 ($[Zn_4O(BDC)_3]_n$), Ali et al. [95] developed a high-performance gas sensor for the low concentration detection of H_2S gas molecules (1 ppm) at room temperature. The sensing components of the device consisted of MOF-5 microparticles, blended and embedded in a conductivity-controlled chitosan organic membrane resulting in the fabrication of a flexible gas sensor (Figure 5f, inset). The sensor demonstrated an increase in the measured current as a linear function of H_2S gas concentration with an LOD of 1 ppm and a fast response and recovery time of 8 s and 30 s, respectively (Figure 5f). This high sensitivity and fast response dynamic were attributed to the synergistic effect of promoted proton conductivity through the membrane matrix and the special cage-bridge structure of MOF-5 (Figure 5g, inset). Such synergistic sensing efforts facilitated the selectivity of MOF-5 embedded sensor towards H_2S gas with a negligible response for other reducing gases at 100 ppm (Figure 5g). The high sensing response of 98% was maintained throughout 21 days of consecutive testing, indicating good repeatability and stability for the fabricated sensor.

The first electronic-textile H_2S gas sensor was reported by Smith et al. [96] through self-organized frameworks on textiles (SOFT) where two conductive 2D MOFs (Ni_3HHTP_2 and Ni_3HITP_2, HITP: 2,3,6,7,10,11-hexaiminotriphenylene) were integrated into cotton by one-step direct solution-phase self-assembly. Using this technique, a high response of 98% and 97% was achieved towards H_2S gas in dry conditions for Ni_3HHTP_2 and Ni_3HITP_2, respectively. Interestingly, a ~26% enhancement in the Ni_3HITP_2 SOFT response was observed by increasing the humidity to 18% RH while Ni_3HITP_2 showed an ~8% reduction in sensing performance under the same conditions. In addition to H_2S gas, the fabricated sensors exhibited high sensitivity towards other gases including nitric oxide (NO) and NH_3 gas, demonstrating wide-ranging potential in the design of novel and multifunctional portable gas sensing devices.

4. Sulphur Dioxide (SO_2)

SO_2 is another toxic air pollutant, posing a serious threat to the environment and human health, with a primary one-hour acceptable limit of 75 ppb set by the U.S. Environmental Protection Agency (EPA) [127]. A wide range of sensing materials, including metal oxide semiconductors [128–130], organic polymers [131], micro-electro-mechanicals (MEMs) [132] and carbon-based nanomaterials [133–136], are employed to develop highly sensitive and selective gas sensors for SO_2 detection. However, their irreversible structural transformation upon exposure to SO_2 hinders their real world application as a practical, reversible gas sensor [130]. Very recently, a series of MOF-based materials, including MOF-74 [137], DMOF-1 (double ligands: 1,4-diazabicyclo[2.2.2]octane and

1,4-benzenedicarboxylic acid) [138] and MFM-300 (MFM: Manchester Framework Material) [100,139] have been reported as promising candidates for SO_2 detection at room temperature. Amongst them, indium-based MOFs, including MFM-300(In), have attracted attention as promising materials for SO_2 detection due to the high SO_2 sorption capacity of up to 8.28 mmol·g^{-1} (at 298 K and 1 bar) and the acceptable stability of coordination compounds to highly reactive SO_2 gas molecules [139].

Recently, Wang et al. [98] synthesised an amino-functionalized luminescent MOF material (MOF-5-NH_2) on a luminescent test paper as a highly sensitive and selective SO_2 gas (and its derivatives) sensor with a short response time of less than 15 s at room temperature. A Kipp's apparatus (Figure 6a) was used to generate the SO_2 gas and control its concentration via tuning the amount of the corresponding acid. The sensing mechanism for this device was based on the interaction between MOF-5-NH_2 and SO_2 molecules, resulting in a change in the absorption/luminescence intensity of the sensing material under UV illumination (λ_{ex} = 365 nm) (Figure 6b). Increasing the concentration of SO_2 from 0 to 3 ppm resulted in a significant increase in the brightness of the luminescent test papers, with an LOD-lightened concentration of 0.05 ppm, suggesting that MOF-5-NH_2 is a promising material for the selective detection of low concentrations of SO_2 at room temperature. In contrast to MOF-5-NH_2, no change was detected in the luminescence intensity of MOF-5 after exposure to SO_2, emphasising the important role that the -NH_2 group plays in the luminescent sensing of MOFs. This observation is in strong agreement with other studies reporting the utilisation of amino-functionalized materials and the selective identification of SO_2 derivatives [140].

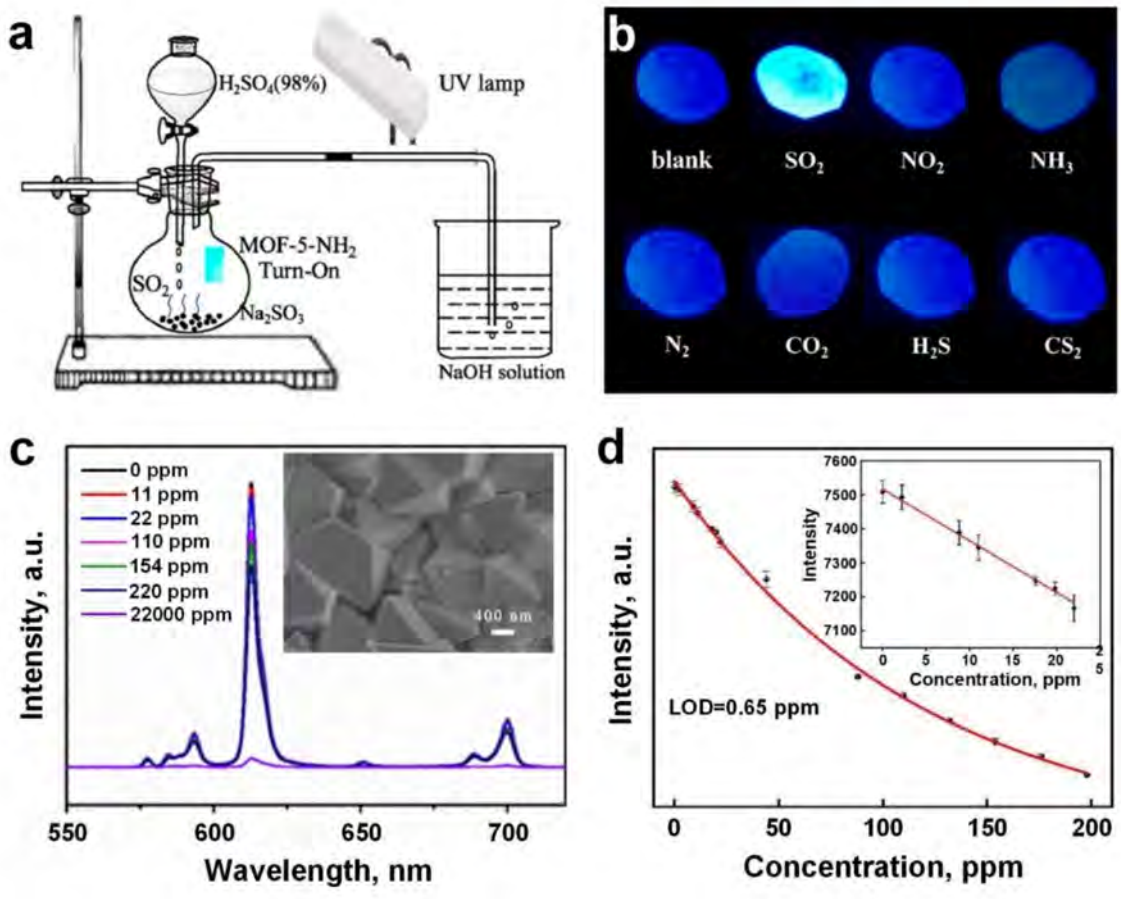

Figure 6. (**a**) Schematic illustration of Kipp's apparatus used for producing SO_2 gas. (**b**) Photographs of MOF-5-NH_2 luminescent test papers upon exposure to different gases (2 ppm concentration) under a 365 nm UV lamp. Reproduced with permission from [98] American Chemical Society, 2018. (**c**) The emission spectra of Eu-BDC-NH_2 film upon exposure to SO_2 gas at different concentrations, and the SEM image of Eu-BDC-NH_2 film (Inset). (**d**) The relationship of fluorescence

intensity versus SO_2 gas for a range of concentrations; the inset displays a linear correlation within a low SO_2 gas concentration range (0–25 ppm). Reproduced with permission from [99] Elsevier, 2018.

In a similar approach, Zhang et al. [99] devised a novel technique of "in situ secondary growth" to readily synthesise Eu-BDC-NH_2 MOF (amino-functionalized) on glass substrates using solvothermally fabricated UiO-66-NH_2 (resulting from the combination of zirconium salt and 2-aminoterephthalic acid (H_2BDC-NH_2); UiO is short for the University of Oslo) as the seed layer for the optical detection of SO_2. As the structure and molecular content of UiO-66-NH_2 crystals are well-matched to Eu-BDC-NH_2, tightly coherent crack-free Eu-BDC-NH_2 films with controllable grain size and film thickness were synthesised (Figure 6c, inset). The fabricated Eu-BDC-NH_2 film was found to exhibit distinctively characteristic Eu^{3+} emissions at 594, 615 and 699 nm under 370 nm excitation within N_2 due to band transition ($^5D_0 \rightarrow {}^7F_J$, J = 1, 2, 4). However, these fingerprint emissions could be significantly suppressed by increasing SO_2 gas concentrations, as depicted in Figure 6c; all emission intensities decreased significantly as SO_2 concentrations were increased from 0 to 220 ppm. The overall emissions were further quenched with a sharp increase in the SO_2 concentration to 22,000 ppm, demonstrating an exponential drop in the luminescence intensity of the sensing materials (Figure 6d). However, at low SO_2 gas concentrations ($\leq$ 25 ppm), a good linear correlation between the two variables was observed (Figure 7d, inset). Meanwhile, the LOD was calculated to be 0.65 ppm, which is significantly lower than the Occupational Safety and Health Administration (OSHA) warning value for SO_2 gas [116].

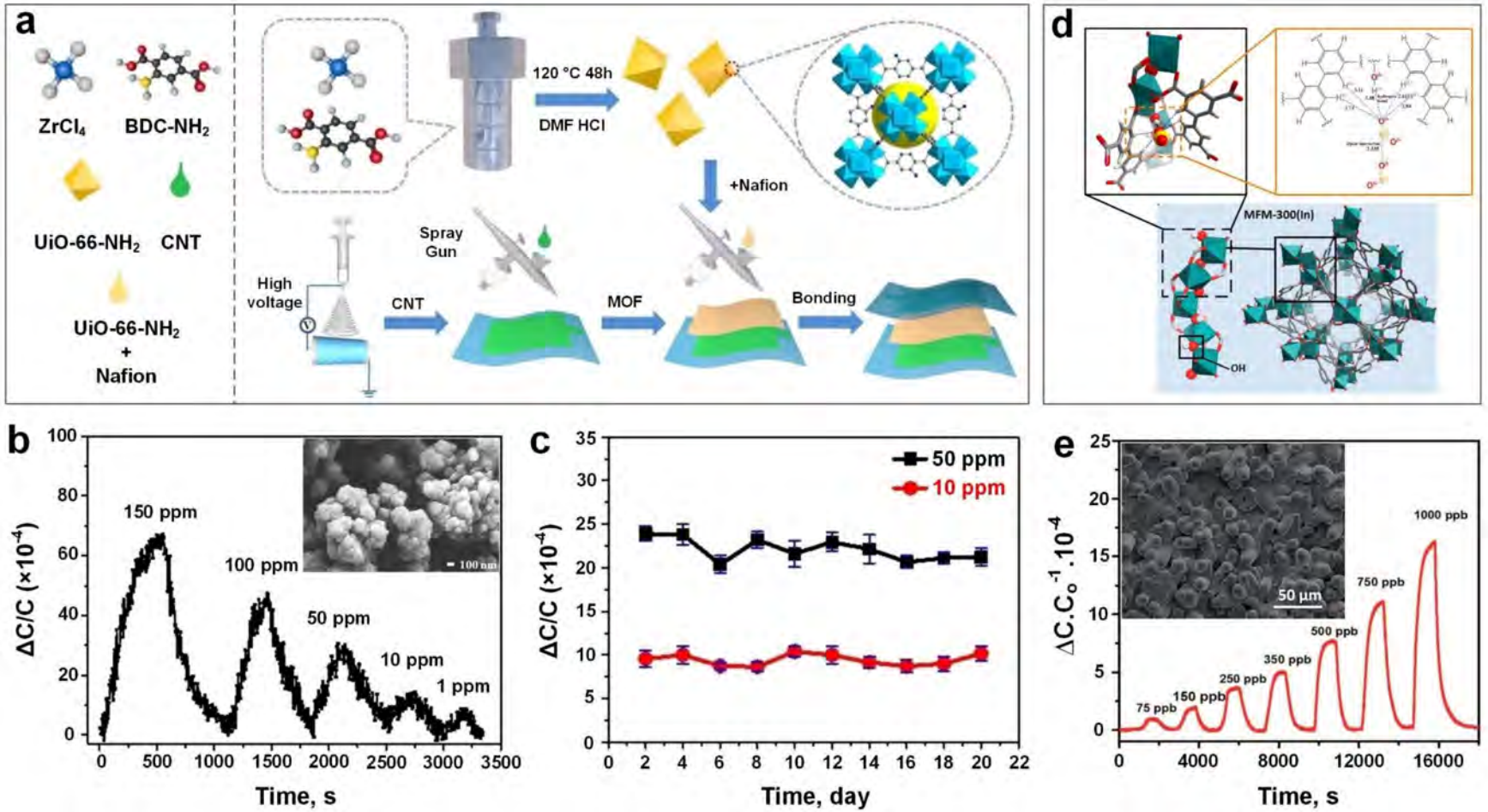

Figure 7. (**a**) Schematic illustrations of UiO-66-NH_2 preparation on flexible PVDF layer for capacitive SO_2 gas sensor. (**b**) The dynamic capacitance variations of UiO-66-NH_2 versus different SO_2 gas concentrations, and the SEM image of UiO-66-NH_2 powder (Inset). (**c**) The stability tests of UiO-66-NH_2 based gas sensor under 10 and 50 ppm of SO_2 gas for over 20 days. Reproduced with permission from [28] Wiley-VCH, 2021. (**d**) The structure of MFM-300 (In) MOF and the sites for SO_2 adsorption. (**e**) The capacitive response of MFM-300 (In) MOF against varied SO_2 gas concentrations, and the SEM image of MFM-300 (In) MOF thin film as inset. Reproduced with permission from [100] The Royal Society of Chemistry, 2018.

Very recently, Zhang et al. [28] developed a capacitive-based sensing material using a relatively simple fabrication process (Figure 7a) for the real-time monitoring of SO_2 gas molecules at room temperature. The sensing technology was introduced by using polyvinylidenefluoride (PVDF) nanofibers (with a diameter of 300–400 nm) coated with a thin layer of UiO-66-NH_2 MOF (200 nm in size) (Figure 7b, inset) as a dielectric layer and carbon nanotubes (CNTs) as an electrode. The fabricated sensing material demonstrated a high sensitivity towards SO_2 in a large ppm range from 1 ppm to 150 ppm (Figure 7b), high stability (over a testing period of 20 days) (Figure 7c) and excellent bending flexibility (2000 bending cycles), with a short response time of 185 s for detecting a low concentration of SO_2 gas. The sensing mechanism was based on the change in the dielectric constant of UiO-66-NH_2 MOF layer due to the physical adsorption of SO_2 gas molecules in the MOF pores and voids. Interestingly, it demonstrated a faster response dynamic (both response and recovery time) after bending (compared to an unbended sample), which could be attributed to the shortened distance between the electrode and dielectric layer, resulting in a shorter transfer path for gas molecules to reach the dialectic layer, and consequently faster response dynamics.

Using a simple solvothermal technique, Chernikova et al. [100] deposited a layer of MFM-300 (a 3-periodic open framework composing of $InO_4(OH)_2$ octahedral chains bridged by tetradentate ligands (biphenyl-3,3′,5,5′-tetracarboxylic acid)) (Figure 7d), on a silicon wafer featuring a capacitive interdigitated electrode functionalized with 11-Mercapto-1-undecanol, for the low concentration detection of SO_2 gas molecules. The sensing performance of the proposed porous nanostructured layer (Figure 7e, inset) was investigated by monitoring the changes in capacitance upon exposure to a selection of different gas molecules including SO_2, CH_4, CO_2, NO_2 and H_2. The results showed outstanding detection sensitivity to SO_2 down to 75 ppb (Figure 6e) with a lower detection limit of 5 ppb and excellent selectivity towards SO_2 compared to other gases with slight cross-selectivity with CO_2 (four times less sensitive compared to SO_2).

The sensing mechanism was based on the interaction between SO_2 molecules and the exposed hydrogen centres from free hydroxyl (OH-) groups on the surface of MFM-300 (Figure 7d), leading to the formation of hydrogen bonds between SO_2 and the sensing materials [100]. Similarly, the neighbouring C-H groups from the benzene ring of the ligand can contribute to SO_2 detection by providing further adsorption sites on the surface (Figure 7d), resulting in excellent sensitivity and selectivity towards SO_2. Interestingly, the adsorbed SO_2 molecules on the surface can interact with each other through analyte-analyte interaction (dipoles), leading to a higher capacitance change in the sensors.

The effect of humidity level on sensing performance of the active film upon SO_2 exposure was investigated at 1000 and 350 ppb gas concentrations, and at relative humidity (RH) from 5% to 85%. In contrast to conventional gas sensors including metal oxide semiconductors, the sensing performance of the MFM-300-based gas sensor was enhanced significantly by increasing the RH up to 85%. This higher sensing response was attributed to the formation of additional hydrogen bonding between SO_2 gas molecules and adsorbed water molecules on the MOF's surface, resulting in a higher capacitance change [107,141]. In addition, the MFM-300 layer demonstrated a higher sensing performance at lower operating temperature with an optimal operating temperature of 22 °C, making it a promising material for highly sensitive, room temperature nanosensors for the ultra-low concentration detection of SO_2 gas molecules. This higher sensitivity could be attributed to a lower molecule diffusion rate and consequently, a higher analyte adsorption rate at a lower temperature [100].

Although the UiO-66(Zr) family of MOFs is unreactive by nature towards acid gases such SO_2, CO_2 and NO_2, functionalising the surface of UiO-66 with an amine moiety can convert it into a chemoresistive acidic gas sensor [101]. The NH_2-OH-UiO-66 exhibited an attractive response of 11.4 ± 2.2% for 10 ppm SO_2 with a fast response and decay time of 26.8 s and 46.1 s, respectively. It was shown that the bandgap of pelletized NH_2-

OH-UiO-66 narrowed down to 2.75 eV compared to the 3.05 eV of Uio-66, indicating an increased charge density at the lowest unoccupied crystalline orbitals (LUCO). Meanwhile, a suggested electron-hopping transport was observed with a decrease of resistance at elevated temperatures. The transformations between a semiconductor and insulator for NH_2-OH-UiO-66 make it an intriguing candidate for SO_2 gas sensing chemoresistively at low concentrations (observed response of 3.2% with concentrations down to 1 ppm). Additionally, NH_2-UiO-66 outperformed the OH-UiO-66(Zr) and NH_2-OH-UiO-66 with approximate 5-fold and 3-fold enhanced responses (4.1% and 7.1% for OH-UiO-66 and NH_2-OH-UiO-66, respectively), highlighting the importance of carefully selecting an appropriate linker for sensing a specific target gas. However, the elevated operating temperature of 150 °C could hinder their applications in practice where room temperature or near room temperature operation is needed.

In another approach, Ingle et al. [102] fabricated a flexible SO_2 gas sensor based on a crystalline nickel (II) benzenetricarboxylate metal-organic framework (Ni-MOF). In this device, the Ni-MOF composited with hydroxyl group (–OH) activated single-wall carbon nanotubes (SWNTs) and multi-wall carbon nanotubes (MWNTs), namely, Ni-MOF/–OH–SWNTs and Ni-MOF/–OH-MWNTs. Both CNT-modified Ni-MOF microdevices exhibited a discriminating response upon SO_2 exposure, which was contributed by the highly sensitive surface network of CNTs [142] providing favourable conditions for electron transportation [143]. The Ni-MOF/–OH-SWNTs sensor showed higher SO_2 sensing performance compared to the Ni-MOF/–OH-MWNTs at different SO_2 concentrations. This was due to holes being the majority charge careers in Ni-MOF/–OH-SWNTs [144] resulting in better interaction with electron donor analytes such as SO_2 gas molecules. However, a slow recovery speed was observed which could be attributed to the honeycomb structure of the CNTs as this plays a significant role in holding the gas molecules on the sensor's surface for a longer time [142,145] prolonging the recovery dynamics of the device. A high sensing selectivity towards SO_2 molecules was also achieved using the MOF/CNT composite material compared to other gases, including NO_2, NH_3 and CO gases, at relatively high concentrations ($\geq$10 ppm).

5. Carbon Dioxide (CO_2)

Despite the modest greenhouse effect of CO_2 compared to methane (CH_4) and nitrous oxide (N_2O), which possess 25 and 298 times more global warming potential (GWP) than CO_2, respectively [146,147], CO_2 is widely understood to be the major driver of climate change due to its dominant concentrations in the atmosphere (0.04 vol%) when compared to other types of greenhouse gas [148]. Sustained exposure to CO_2 gas indoors can cause inflammation and oxidative stress at a modest concentration level of 1000 ppm [149,150]. Thus, ongoing monitoring of indoor and outdoor CO_2 gas levels with reliable, portable and cost-effective sensing systems is highly desired in many industrial sectors.

Recently, a novel sensing mechanism was introduced to leverage small molecules by extremely small differences in the refractive indices (RI) of MOF nanofilms as a function of analyte adsorption within a MOF layer. This allows for the detection of chemical compounds at the molecular level via slight distinctions in refractive index (RI) through utilization of an optical-fiber-waveguide framework (Figure 8a(i)). Using a simple solution-based technique, Kim et al. [103] synthesised a uniform, dense and continuous layer of ZIF-8 around an etched fiber optical sensor (Figure 8a(ii,iii)) for low concentration detection of CO_2 gas molecules at room temperature. The transmittance of the ZIF-8 coated optical fibre at the wavelength of 242 nm decreased by a factor of 2 from 100% to 50% by increasing the concentration of CO_2 gas molecules from zero to 100% (Figure 8b), indicating a linear relationship between the sensing response and the concentration of CO_2 gas (Figure 8b, inset). The sensing mechanism is based on a shift in the RI of the ZIF-8 layer due to the adsorption of CO_2 gas molecules into the MOF apertures. According to the Lorenz−Lorentz law, the density of ZIF-8 film increases when CO_2 gas molecules are adsorbed on the surface, resulting in a change in the RI of the MOF layer. This RI change in

the MOF layer is proportional to the number of CO_2 molecules adsorbed on the surface. Hence, the closer the RI of the MOF layer is to the RI of the fibre, the more light propagates from the fibre optic into the MOF film, resulting in lower transmittance at the wavelength of 242 nm [103].

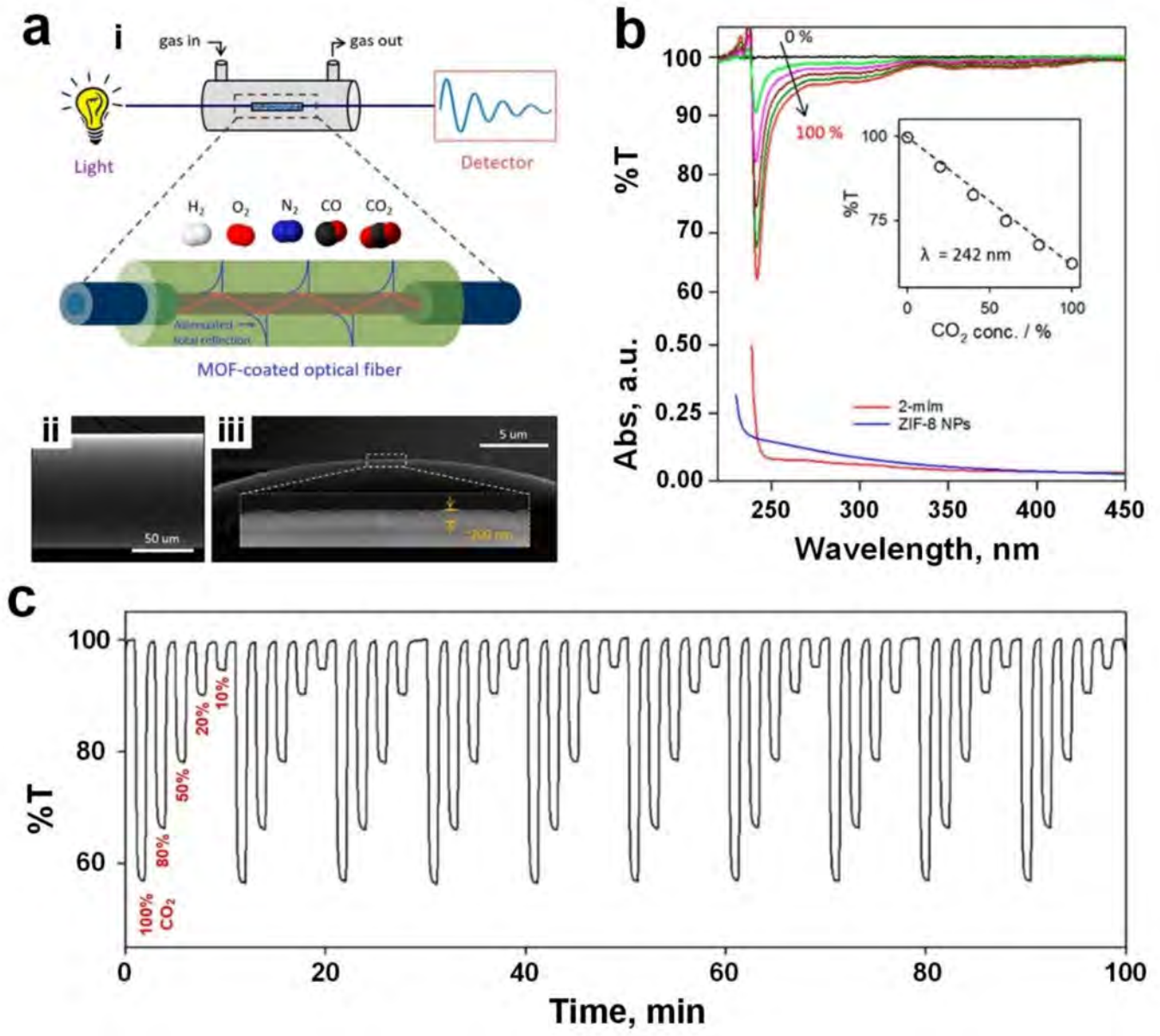

Figure 8. (**a**(i)) Graphic representation of the gas detection system using MOF-coated optical fiber. FESEM images of top (**a**(ii)) and side (**a**(iii)) views of optical fiber covered by 200 nm thick ZIF-8. (**b**) The transmittance spectra of 350 nm thick ZIF-8 coated optical fiber against varied CO_2 levels, and the absorbance spectra of 2-mIm and ZIF-8. A linearity of %T (λ = 242 nm) and CO_2 concentrations was plotted as inset. (**c**) Ten cyclic dynamic responses of 200 nm thick ZIF-8 coated optical fiber under different CO_2 concentrations. Reproduced with permission from [103] American Chemical Society, 2018.

This lower transmittance was mainly due to a significant absorbance wavelength (λ = 242 nm) induced by the 2-methylimidazole linker within the ZIF-8 layer, as indicated by the observed similarity with the maximum absorbance wavelength obtained for the free 2-methylimidazole linker in the diluted fluid (Figure 8b). At wavelengths over 250 nm, the changes in transmittances are negligible due to the weak 2-methylimidazole absorption band trail at longer wavelengths (Figure 8b) [103]. This sensing technology demonstrated a remarkably fast response and recovery time of 14 s and 9 s, respectively, for 200 nm

thick ZIF-8 film. However, the response and recovery times increased to 84 and 24 s, respectively, by increasing the ZIF-8 film thickness to 530 nm. This slower response dynamic could be attributed to the long-range diffusion rate of gas transferring through the ZIF-8 crystallites toward the interior of the film. In addition, excellent repeatability (Figure 8c) and high selectivity towards CO_2 gas molecules were observed compared to other gases with relatively small molecule sizes, including H_2, N_2, O_2, and CO.

Using an in situ solvothermal technique, Yuan et al. [9] fabricated a tailorable capacitive sensor for selective detection of benzene vapour and CO_2 gas molecules at room temperature. The sensor was made of Mg-MOF-74 crystallites grown on a silicon nitride (Si_3N_4) substrate featuring platinum (Pt) IDEs (Figure 9a,b). By changing the metal ion (Mg) to linker (2,5-dioxido-1,4-benzenedicarboxylate (DOBDC)) ratio (κ) for the MOF growth, a thick (7 μm) and compact film morphology with intergrown hexagonal crystallites (Figure 9c,d) was observed for $\kappa > 3$, compared to isolated hexagonal bunches with free space on the substrate for $\kappa < 2$. This change in the morphology is attributed to the competition between the simultaneous homogeneous and heterogeneous nucleation and growth of the Mg-MOF-74 films. The homogeneous (in solution) nucleation was dominant at a lower κ where a higher concentration of ligand led to precursor consumption, powder formation and, consequently, growth restriction, and resultant formation of additional voids on the surface. In contrast, the nucleation was limited at a higher κ where heterogenous (on surface) growth was promoted, resulting in the formation of highly intergrown crystallites forming a dense and compact layer (Figure 9d).

The sensing performance of the MOF film was investigated by measuring the capacitance change upon exposure to different gases including methane, benzene and CO_2, resulting in an outstanding sensing response of ~1 towards 200 ppm CO_2 vapour (Figure 9e). This response is attributed to the interaction between unsaturated open metal sites of the Mg-MOF-74 crystallites (as an electron acceptor) and adsorbed CO_2 molecules acting as electron donors. A positive linear response was reported upon increasing the CO_2 gas concentration from 200 to 5000 ppm and attributed to the linear change in the dielectric constant of the Mg-MOF-74 layer over the gas adsorption on the surface (Figure 9e, inset). However, no obvious response was detected for other gases, including methane, at similar concentrations. Post-synthesis modification of these MOF layers with ethylenediamine slightly increased their sensitivity towards CO_2. However, further investigations are required to reveal the key factors in the sensing performance of Mg-MOF-74 crystallites and their surface-analyte interaction with different gas molecules.

Inspired by the Guest@MOF concept which combines MOFs and guest molecules to prompt the conductivity of MOF [151], Strauss et al. [152] designed a chemoresistive gas sensor based on one-dimensional Co-MOF-74-TTF (Figure 9f, inset) materials. This was achieved by infiltration of Co-MOF-74 (with Co as the metallic centre linked by 2,5-dioxido-1,4-benzenedicarboxylate ligands) powder with the organic semiconductor tetrathiafulvalene (TTF) [152]. As presented in Figure 9f, a significant increase in the CO_2 uptake (up to 100 $cc \cdot g^{-1}$) was observed when the CO_2 pressure inside the cell was increased stepwise up to 1000 mbar. In contrast, the CO_2 uptake only increased up to ~18 $cc \cdot g^{-1}$ for Co-MOF-74-TTF after increasing the CO_2 pressure to 1000 mbar. This lower CO_2 uptake could be attributed to the blockage of pore volumes in Co-MOF-74-TTF. In fact, the amount of adsorbed CO_2 was drastically reduced in Co-MOF-74-TTF because of the TTF molecules infiltrated into the pores (i.e., successful infiltration).

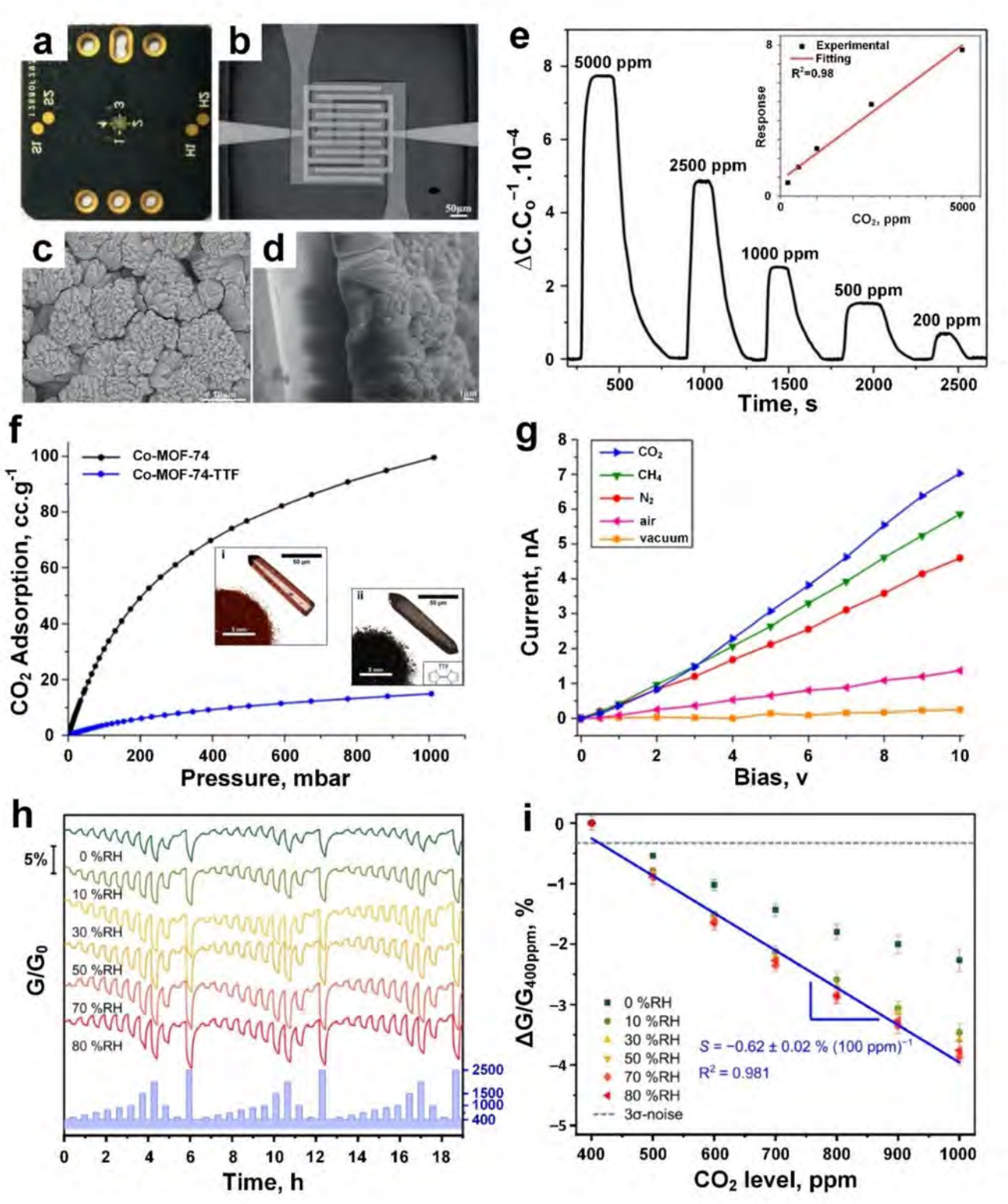

Figure 9. (**a**) Photograph of Mg-MOF-74 film-based CO_2 capacitive gas sensor. (**b**) Optical image of Pt IDEs. (**c**,**d**) SEM images of the top (**c**) and side (**d**) views of the as-grown Mg-MOF-74 film on IDEs. (**e**) The dynamic response of ethylenediamine-modified Mg-MOF-74 film against CO_2 at different concentrations, the response varied proportionally to the CO_2 concentration (inset). Reproduced with permission from [9] Wiley-VCH, 2019. (**f**) CO_2 adsorption isotherms of Co-MOF-74 (i) and Co-MOF-74-TTF (ii). (**g**) The *I-V* curves of Co-MOF-74-TTF under CO_2 and other atmospheric conditions. Reproduced with permission from [152] American Chemical Society, 2019. (**h**) The normalized dynamic response curves and, (**i**) response versus CO_2 gas at different concentrations for various humidity scenarios (0−80% RH). Reproduced with permission from [104] American Chemical Society, 2019.

To investigate the gas-sensing capability of Co-MOF-74-TTF, the *I-V* characteristics of the sensing material was measured after 24 h under vacuum, air, N_2, CH_4, and CO_2 atmospheres, respectively, at an applied voltage up to 10 V. The material demonstrated a higher sensing performance towards CO_2 gas molecules (current of 7 nA) compared to other gases including CH_4 (current of 6 nA) and N_2 (current of 4.5 nA) at 10 V (Figure 9g). This higher sensing performance could be attributed to the strong interaction between open-metal Co-centres (acting as the Lewis acid) of MOF and CO_2 gas molecules (acting as the Lewis base/electron donor) resulting in the highest conductivity of the fabricated sensing material upon exposure to CO_2 gas (Figure 9g), while a smaller increase in the conductivity was observed for weaker gas−MOF interactions ($CO_2 > CH_4 > N_2$). In fact, the permanent dipole moment, which is present in the cobalt atoms, could induce the polarization of molecules such as CH_4, resulting in the lower affinity of Co-MOF-74 toward CH_4 compared to CO_2 [153]. In addition, a significantly lower interaction was expected for N_2, as an inert gas, resulting in a lower sensing response towards N_2 gas molecules. Further investigation is required to resolve the poor selectivity and slow response dynamics (>500 min) of these Co-MOF-74-TTF for their real-world application as CO_2 gas sensors [152].

In another approach, Stassen et al. [104] reported the fabrication of an ambient CO_2 chemoresistor platform based on nanoporous, electrically conducting 2D MOFs deposited on Al_2O_3 substrates featuring IDEs. The normalized response dynamics of the fabricated sensing MOFs (Cu_3(hexaiminobenzene)$_2$, $Cu_3(HIB)_2$) at different CO_2 concentrations (400−2500 ppm) demonstrated a highly repeatable and robust operation over 7 days of continuous experimentation and remarkable humidity-independence across a wide range of relative humidity (10−80% RH) (Figure 9h). Figure 9i shows the quantitative responses of the sensing material upon exposure to CO_2 gas molecules across a concentration range of 400 to 1000 ppm, demonstrating a linear response-concentration relationship and an average response of 0.62%/100 ppm over the broad range of ambient humidity (10−80% RH). This strong RH-independency of the $Cu_3(HIB)_2$ senor towards CO_2 gas molecules could be attributed to the autogenously generated hydrated adsorption sites and a charge trap mechanism of $Cu_3(HIB)_2$ resulting in such intriguing CO_2 sensing performance at high RH, outperforming other amine-rich based CO_2 sensors including polyethylenimine (PEI) [154] and ZIF-8 [155–157]. This indicates the great potential of $Cu_3(HIB)_2$-based MOFs as remarkably stable sensing materials for real-world applications in a highly humid environment.

6. Ammonia (NH_3)

Ammonia is one of the most important gases present in human activities, especially in relation to its use in agriculture, where nitrogenous fertilizers are extensively used. It is a corrosive and flammable gas with a pungent smell and an odour threshold range of 5−50 ppm. Exposure to a large quantity of NH_3 (concentrations greater than 300 ppm) can cause burns to the eyes and skin and can damage the respiratory system [158]. In addition, NH_3 is a natural product produced in the human body by various metabolic activities and is a promising breath biomarker for the well-being of patients with kidney and liver diseases [159,160]. Thus, the development of a non-invasive, flexible, reliable, robust and fast NH_3 gas sensors operating at a low temperature is of great interest.

A luminescent quantitative-based sensor for NH_3 gas detection fabricated by in situ solvothermal growth of MOF film (MIL-124@Eu^{3+}, where MIL-124(In) was first synthesised by mixture of $InCl_3$ and 1,2,4-benzenetricarboxylic acid, followed by immersion into Eu^{3+} solution for preparation of the final product) on a porous α-Al_2O_3 substrate [106]. This sensor demonstrated an outstanding sensing threshold of 26.2 ppm, which is significantly lower than the OSHA-specified health alert line of 50 ppm. The sensing mechanism was based on the partial coordination of carboxylates on the surface of MIL-124@Eu^{3+}, leaving free -COOH to serve as active sites for NH_3 interaction to form -$COONH_4$. The formation of -$COONH_4$ changes the energy transfer process between ligand and Eu^{3+} ions,

leading to the quenching effect of luminescence emission of MIL-124@Eu^{3+} film upon exposure to NH_3 gas molecules.

In chemoresistors, using a rapid (<16 min) interfacial self-assembly method (Figure 10a), Chen et al. [108] synthesised a centimetre-sized conductive MOF film (copper benzenehexathiol, Cu-BHT) for highly sensitive and selective detection of NH_3 gas molecules at room temperature. Due to the rapid interaction between Cu^{2+} and BHT ligands usingsuch as in situ synthesis technique (Figure 10b), the Cu-BHT film was formed at the interface between $Cu(NO_3)_2$ aqueous solution and BHT organic solution within 5 s. A continuous and uniform Cu-BHT film was then prepared by spinning the solution off at high speed. The film thickness could be controlled by tuning the reaction time, resulting in more coordination reactions, and consequently thicker film for an extended reaction time. Figure 10b shows the crystal structure of Cu-BHT, where Cu ions are coordinated by BHT ligands to form a 2D kagome lattice structure with an interval distance of 3.38 Å.

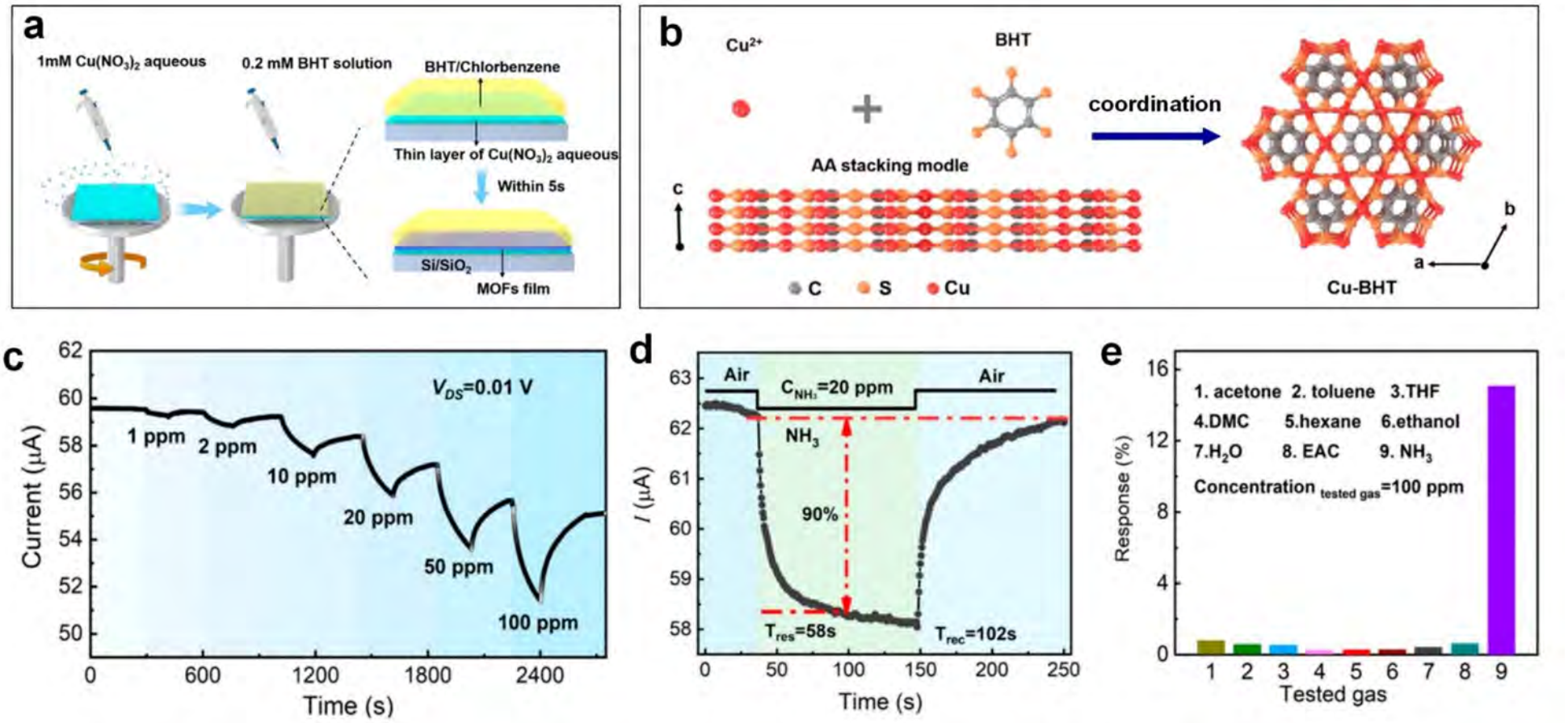

Figure 10. (**a**) Schematic illustrations of ultrafast in situ synthesis of large-area Cu-BHT on Si/SiO_2 substrate. (**b**) Demonstrations of Cu-BHT crystalline structure and AA stacking model. (**c**) The dynamic current variations under different NH_3 concentrations. (**d**) Response kinetics of Cu-BHT film towards 20 ppm NH_3. (**e**) Cross-selectivity of Cu-BHT film towards various reducing gases with the concentration of 100 ppm. Reproduced with permission from [108] American Chemical Society, 2021.

A 10-nm-thick Cu-BHT thin-film demonstrated an excellent sensing performance towards NH_3 gas molecules (Figure 10c) with a sensing response of ~16% upon exposure to 100 ppm NH_3 and under a low driving voltage of 0.01 V (Figure 10e). This high sensitivity was 30–50 times higher compared to other gases including acetone, toluene and hexane, indicating strong selectivity towards the target gas (Figure 10e). In addition, a remarkable LOD of 0.23 ppm and fast signal dynamic of 58 s and 102 s for response and recovery time, respectively, was recorded for NH_3 gas with 20 ppm concentration (Figure 10d). However, the gas sensing performance dropped from 7.88% to 4.01% by increasing the RH from 0 to 80%, due to sensing site blockage by water vapour molecules. Thus, surface modifications, including integration of hydrophobic MOFs fillers (e.g., microporous MIL-160/PDMS [161]) on the surface of Cu-BHT via Van der Waals interactions, are likely to significantly improve the sensing performance in a high humidity environment [162].

In another approach, a 2D conductive MOF-based sensor, namely, $Cu_3(HITP)_2$, was synthesised by a drop-casting technique for sub-ppm detection of NH_3 gas molecules under an applied bias of 0.1 V [109]. The fabricated sensor demonstrated a linear response with increasing concentration of NH_3 gas from 0.5 to 10 ppm, indicating that $Cu_3(HITP)_2$ is a promising candidate for the quantitative sensing of NH_3 at a wide range of concentrations. Very recently, Khan et al. [111] reported the synthesis of Pd-Co@MOF-5 core-shell nanocomposite as a fast, highly sensitive, and selective gas sensor for sub-ppm detection of NH_3 at room temperature. The nanocomposite sensor exhibited remarkable resistive signals upon exposure to ammonia gas molecules in the range of 1 to 90 ppm concentration of NH_3. The sensor's response increased linearly from 1.5 for 1 ppm concentration to 80.17 for 90 ppm concentration with a fast response dynamic of 46 s and 22 s for response and recovery time, respectively. This excellent sensing performance towards NH_3 could be attributed to the rich open/unsaturated metal sites in the porous MOF-5 structure and the surface carboxyl group providing extra absorption sites for ammonia interaction. In addition to high sensitivity, an excellent selectivity towards NH_3 was reported with negligible response to other gases including ethanol, formaldehyde, acetone and benzene at the same gas concentration (90 ppm).

Most recently, a Cu-HHTP 3D thin film (20 nm in thickness) was prepared in a controllable layer-by-layer approach for NH_3 gas sensing at room temperature [110]. Instead of using a flat substrate for MOF growth, a TiO_2 nanowire array (NWAs) was grown on sapphire hydrothermally providing a large surface area, short charge and mass transport pathway. The fabricated films exhibited a response of 1.6 towards 100 ppm NH3 gas with a fast response time of 35 s. This was 600% and 130% faster compared to Cu-HHTP powder and 2D thin film with the same thickness, respectively. A record low LOD of ~87 ppt and an excellent selectivity among the most common carbonaceous gases (such as CO_2, CO, CH_4, EtOH, MeOH, acetone, etc.) and H_2 was achieved. Such a high sensing performance at room temperature casts a bright light on NH_3 gas sensing design. However, further work is encouraged to promote faster recovering kinetics as a 15 min recovery time impedes the potential of Cu-HHTP 3D thin film for practical applications.

7. Summary and Outlook

In summary, we have reviewed and discussed in detail recent advances in the development of MOF-based nanosensors for air quality and environmental monitoring applications. In this comprehensive review, the main focus has been on the most recent research progress in capacitive, optical and chemoresistive sensors made of MOF nanoparticles and nanofilms. The sensing performance, along with the corresponding sensing mechanisms of the state-of-the-art technologies, was carefully investigated for the room temperature detection of gases including NO_2, SO_2, H_2S, CO_2 and NH_3 with a wide variety of MOF-based nanosensing technologies.

High sensitivity and selectivity at low operating temperatures have been reported for state-of-the-art MOF-based sensors making them a promising candidate for various

gas-sensing applications; however, MOF-based nanosensors for sub-ppb detection of gas molecules are still in the initial stages of development, with much room to improve the sensing performance of these MOF materials and many opportunities to enhance their LODs towards gas molecules.

High chemical, thermal, and photo stabilities have been achieved for some of the MOF-based sensing technologies, which determine their repeatability and long-term reusability. However, recent studies have indicated that some of the widely used MOFs for gas sensors undergo partial degradation upon exposure to moisture. Continued efforts are necessary for the design and development of robust MOF-based sensing materials to demonstrate long-term stability in different environments. Careful assessment of MOF sensors after long-term tests using analytical techniques sensitive to MOF degradation will enable researchers to improve their stability. The careful design of novel MOF structures (such as mixed metal ions, hydrophobic ligands, and interpenetration of frameworks), post-processing of current MOFs (such as metal/ligand exchange, hydrophobic surface modification, and thermal treatment), and compositing MOFs with, or encapsulating MOFs into, other materials (such as polymers, carbon nanotubes, graphenes and graphene oxide) are among the proposed techniques for improving the chemical stability of MOFs.

Among several different fabrication techniques, the solvothermal method is the most common synthesis method to produce MOF particles which are then incorporated into the sensing devices using drop coating, spin coating, electrospinning, etc. Despite the progress in nanofabrication methodologies, there have been limited investigations that consider environmentally friendly synthesis techniques to form MOFs for gas-sensing purposes using a green approach with high yield, hence minimum wastes [69,70]. Fabrication of MOFs through a green and scalable route is of great importance to their commercial translation and real-life application.

The inherently low electrical conductivity of most MOFs has severely limited their applications in gas and liquid sensors. However, the development of highly porous 2D conductive MOFs with tunable cavity size has facilitated the rise of MOF-based sensing technologies. In addition, the design of novel nanomaterials, including guest-MOF nanostructures where MOFs and guest molecules are combined, has shown excellent enhancement in the conductivity of MOF-based gas sensors.

The future is bright for the development of highly sensitive and selective MOF-based nanosensors for room temperature detection of low concentrations of gas molecules, with applications in many areas of technology, industry, or daily life, providing strong health, safety and security benefits to address many standing fundamental and technological challenges.

Funding: This research received no external funding.

Institutional Review Board Statement: Not applicable.

Informed Consent Statement: Not applicable.

Data Availability Statement: Not applicable.

Conflicts of Interest: The authors declare no conflict of interest.

References

1. Lustig, W.P.; Mukherjee, S.; Rudd, N.D.; Desai, A.V.; Li, J.; Ghosh, S.K. Metal–organic frameworks: Functional luminescent and photonic materials for sensing applications. *Chem. Soc. Rev.* **2017**, *46*, 3242–3285. [CrossRef]
2. Fang, X.; Zong, B.; Mao, S. Metal–Organic Framework-Based Sensors for Environmental Contaminant Sensing. *Nano-Micro Lett.* **2018**, *10*, 64. [CrossRef] [PubMed]
3. Zhou, X.; Xue, Z.; Chen, X.; Huang, C.; Bai, W.; Lu, Z.; Wang, T. Nanomaterial-based gas sensors used for breath diagnosis. *J. Mater. Chem. B* **2020**, *8*, 3231–3248. [CrossRef]
4. Nasiri, N.; Clarke, C. Nanostructured Gas Sensors for Medical and Health Applications: Low to High Dimensional Materials. *Biosensors* **2019**, *9*, 43. [CrossRef]
5. Nasiri, N.; Clarke, C. Nanostructured Chemiresistive Gas Sensors for Medical Applications. *Sensors* **2019**, *19*, 462. [CrossRef] [PubMed]

6. Chen, X.; Leishman, M.; Bagnall, D.; Nasiri, N. Nanostructured Gas Sensors: From Air Quality and Environmental Monitoring to Healthcare and Medical Applications. *Nanomaterials* **2021**, *11*, 1927. [CrossRef]
7. Korotcenkov, G.; Cho, B.K. Metal oxide composites in conductometric gas sensors: Achievements and challenges. *Sens. Actuators B Chem.* **2017**, *244*, 182–210. [CrossRef]
8. Li, H.-Y.; Zhao, S.-N.; Zang, S.-Q.; Li, J. Functional metal-organic frameworks as effective sensors of gases and volatile compounds. *Chem. Soc. Rev.* **2020**, *49*, 6364–6401. [CrossRef] [PubMed]
9. Yuan, H.; Tao, J.; Li, N.; Karmakar, A.; Tang, C.; Cai, H.; Pennycook, S.J.; Singh, N.; Zhao, D. On-Chip Tailorability of Capacitive Gas Sensors Integrated with Metal–Organic Framework Films. *Angew. Chem.* **2019**, *131*, 14227–14232. [CrossRef]
10. Wang, H.; Lustig, W.P.; Li, J. Sensing and capture of toxic and hazardous gases and vapors by metal–organic frameworks. *Chem. Soc. Rev.* **2018**, *47*, 4729–4756. [CrossRef]
11. Rasheed, T.; Nabeel, F. Luminescent metal-organic frameworks as potential sensory materials for various environmental toxic agents. *Coord. Chem. Rev.* **2019**, *401*, 213065. [CrossRef]
12. Wenger, O.S. Vapochromism in Organometallic and Coordination Complexes: Chemical Sensors for Volatile Organic Compounds. *Chem. Rev.* **2013**, *113*, 3686–3733. [CrossRef]
13. Dolgopolova, E.A.; Rice, A.M.; Martin, C.R.; Shustova, N.B. Photochemistry and photophysics of MOFs: Steps towards MOF-based sensing enhancements. *Chem. Soc. Rev.* **2018**, *47*, 4710–4728. [CrossRef] [PubMed]
14. Yan, B. Lanthanide-Functionalized Metal–Organic Framework Hybrid Systems to Create Multiple Luminescent Centers for Chemical Sensing. *Acc. Chem. Res.* **2017**, *50*, 2789–2798. [CrossRef]
15. Wang, X.-D.; Wolfbeis, O.S. Optical methods for sensing and imaging oxygen: Materials, spectroscopies and applications. *Chem. Soc. Rev.* **2014**, *43*, 3666–3761. [CrossRef] [PubMed]
16. Dey, A. Semiconductor metal oxide gas sensors: A review. *Mater. Sci. Eng. B Solid-State Mater. Adv. Technol.* **2018**, *229*, 206–217. [CrossRef]
17. Hu, Z.; Deibert, B.J.; Li, J. Luminescent metal–organic frameworks for chemical sensing and explosive detection. *Chem. Soc. Rev.* **2014**, *43*, 5815–5840. [CrossRef]
18. Karmakar, A.; Samanta, P.; Desai, A.V.; Ghosh, S.K. Guest-Responsive Metal–Organic Frameworks as Scaffolds for Separation and Sensing Applications. *Acc. Chem. Res.* **2017**, *50*, 2457–2469. [CrossRef]
19. Stassen, I.; Burtch, N.; Talin, A.; Falcaro, P.; Allendorf, M.; Ameloot, R. An updated roadmap for the integration of metal–organic frameworks with electronic devices and chemical sensors. *Chem. Soc. Rev.* **2017**, *46*, 3185–3241. [CrossRef]
20. Wales, D.J.; Grand, J.; Ting, V.P.; Burke, R.D.; Edler, K.J.; Bowen, C.R.; Mintova, S.; Burrows, A.D. Gas sensing using porous materials for automotive applications. *Chem. Soc. Rev.* **2015**, *44*, 4290–4321. [CrossRef]
21. Kreno, L.E.; Leong, K.; Farha, O.K.; Allendorf, M.; Van Duyne, R.P.; Hupp, J.T. Metal–Organic Framework Materials as Chemical Sensors. *Chem. Rev.* **2012**, *112*, 1105–1125. [CrossRef]
22. Reglero Ruiz, J.; Sanjuán, A.; Vallejos, S.; García, F.; García, J. Smart Polymers in Micro and Nano Sensory Devices. *Chemosensors* **2018**, *6*, 12. [CrossRef]
23. Ciprian, R.; Baratto, C.; Giglia, A.; Koshmak, K.; Vinai, G.; Donarelli, M.; Ferroni, M.; Campanini, M.; Comini, E.; Ponzoni, A.; et al. Magnetic gas sensing exploiting the magneto-optical Kerr effect on ZnO nanorods/Co layer system. *RSC Adv.* **2016**, *6*, 42517–42521. [CrossRef]
24. Matatagui, D.; Kolokoltsev, O.V.; Qureshi, N.; Mejía-Uriarte, E.V.; Saniger, J.M. A magnonic gas sensor based on magnetic nanoparticles. *Nanoscale* **2015**, *7*, 9607–9613. [CrossRef] [PubMed]
25. Zou, C.W.; Wang, J.; Liang, F.; Xie, W.; Shao, L.X.; Fu, D.J. Large-area aligned CuO nanowires arrays: Synthesis, anomalous ferromagnetic and CO gas sensing properties. *Curr. Appl. Phys.* **2012**, *12*, 1349–1354. [CrossRef]
26. Impeng, S.; Junkaew, A.; Maitarad, P.; Kungwan, N.; Zhang, D.; Shi, L.; Namuangruk, S. A MnN_4 moiety embedded graphene as a magnetic gas sensor for CO detection: A first principle study. *Appl. Surf. Sci.* **2019**, *473*, 820–827. [CrossRef]
27. Zhu, C.; Gerald, R.E.; Huang, J. Metal-organic Framework Materials Coupled to Optical Fibers for Chemical Sensing: A Review. *IEEE Sens. J.* **2021**, 1. [CrossRef]
28. Zhang, X.; Zhai, Z.; Wang, J.; Hao, X.; Sun, Y.; Yu, S.; Lin, X.; Qin, Y.; Li, C. Zr-MOF Combined with Nanofibers as an Efficient and Flexible Capacitive Sensor for Detecting SO_2. *ChemNanoMat* **2021**. [CrossRef]
29. Zhai, Z.; Zhang, X.; Hao, X.; Niu, B.; Li, C. Metal–Organic Frameworks Materials for Capacitive Gas Sensors. *Adv. Mater. Technol.* **2021**, 2100127. [CrossRef]
30. Fernandez, E.; Saiz, P.G.; Peřinka, N.; Wuttke, S.; Fernández De Luis, R. Printed Capacitive Sensors Based on Ionic Liquid/Metal-Organic Framework Composites for Volatile Organic Compounds Detection. *Adv. Funct. Mater.* **2021**, *31*, 2010703. [CrossRef]
31. Srinivas, C.; Ranjith Kumar, E.; Tirupanyam, B.V.; Singh Meena, S.; Bhatt, P.; Prajapat, C.L.; Chandrasekhar Rao, T.V.; Sastry, D.L. Study of magnetic behavior in co-precipitated Ni–Zn ferrite nanoparticles and their potential use for gas sensor applications. *J. Magn. Magn. Mater.* **2020**, *502*, 166534. [CrossRef]
32. Sava Gallis, D.F.; Vogel, D.J.; Vincent, G.A.; Rimsza, J.M.; Nenoff, T.M. NO_x Adsorption and Optical Detection in Rare Earth Metal–Organic Frameworks. *ACS Appl. Mater. Interfaces* **2019**, *11*, 43270–43277. [CrossRef]
33. Chen, H.; Bo, R.; Shrestha, A.; Xin, B.; Nasiri, N.; Zhou, J.; Di Bernardo, I.; Dodd, A.; Saunders, M.; Lipton-Duffin, J.; et al. NiO–ZnO Nanoheterojunction Networks for Room-Temperature Volatile Organic Compounds Sensing. *Adv. Opt. Mater.* **2018**, *6*, 1800677. [CrossRef]

34. Gerber, A.; Kopnov, G.; Karpovski, M. Hall effect spintronics for gas detection. *Appl. Phys. Lett.* **2017**, *111*, 143505. [CrossRef]
35. Alam, M.F.B.; Phan, D.-T.; Chung, G.-S. Palladium nanocubes decorated on a one-dimensional ZnO nanorods array for use as a hydrogen gas sensor. *Mater. Lett.* **2015**, *156*, 113–117. [CrossRef]
36. Yang, S.; Lei, G.; Xu, H.; Lan, Z.; Wang, Z.; Gu, H. Metal Oxide Based Heterojunctions for Gas Sensors: A Review. *Nanomaterials* **2021**, *11*, 1026. [CrossRef]
37. Zhang, J.; Qin, Z.; Zeng, D.; Xie, C. Metal-oxide-semiconductor based gas sensors: Screening, preparation, and integration. *Phys. Chem. Chem. Phys.* **2017**, *19*, 6313–6329. [CrossRef] [PubMed]
38. Cichosz, S.; Masek, A.; Zaborski, M. Polymer-based sensors: A review. *Polym. Test.* **2018**, *67*, 342–348. [CrossRef]
39. Fratoddi, I.; Venditti, I.; Cametti, C.; Russo, M.V. Chemiresistive polyaniline-based gas sensors: A mini review. *Sens. Actuators B Chem.* **2015**, *220*, 534–548. [CrossRef]
40. Ding, B.; Yamazaki, M.; Shiratori, S. Electrospun fibrous polyacrylic acid membrane-based gas sensors. *Sens. Actuators B Chem.* **2005**, *106*, 477–483. [CrossRef]
41. Barauskas, D.; Pelenis, D.; Vanagas, G.; Viržonis, D.; Baltrušaitis, J. Methylated Poly(ethylene)imine Modified Capacitive Micromachined Ultrasonic Transducer for Measurements of CO_2 and SO_2 in Their Mixtures. *Sensors* **2019**, *19*, 3236. [CrossRef]
42. Gargiulo, V.; Alfano, B.; Di Capua, R.; Alfé, M.; Vorokhta, M.; Polichetti, T.; Massera, E.; Miglietta, M.L.; Schiattarella, C.; Di Francia, G. Graphene-like layers as promising chemiresistive sensing material for detection of alcohols at low concentration. *J. Appl. Phys.* **2018**, *123*, 024503. [CrossRef]
43. Li, C.; Wang, Y.; Jiang, H.; Wang, X. Review—Intracellular Sensors Based on Carbonaceous Nanomaterials: A Review. *J. Electrochem. Soc.* **2020**, *167*, 037540. [CrossRef]
44. Wang, Y.; Yeow, J.T.W. A Review of Carbon Nanotubes-Based Gas Sensors. *J. Sens.* **2009**, *2009*, 493904. [CrossRef]
45. Zhang, T.; Mubeen, S.; Myung, N.V.; Deshusses, M.A. Recent progress in carbon nanotube-based gas sensors. *Nanotechnology* **2008**, *19*, 332001. [CrossRef]
46. Llobet, E. Gas sensors using carbon nanomaterials: A review. *Sens. Actuators B Chem.* **2013**, *179*, 32–45. [CrossRef]
47. Lee, J.M.; Park, J.-E.; Kim, S.; Kim, S.; Lee, E.; Kim, S.-J.; Lee, W. Ultra-sensitive hydrogen gas sensors based on Pd-decorated tin dioxide nanostructures: Room temperature operating sensors. *Int. J. Hydrog. Energy* **2010**, *35*, 12568–12573. [CrossRef]
48. Sharma, B.; Kim, J.-S. Graphene decorated Pd-Ag nanoparticles for H_2 sensing. *Int. J. Hydrog. Energy* **2018**, *43*, 11397–11402. [CrossRef]
49. Zhang, S.; Yang, M.; Liang, K.; Turak, A.; Zhang, B.; Meng, D.; Wang, C.; Qu, F.; Cheng, W.; Yang, M. An acetone gas sensor based on nanosized Pt-loaded Fe_2O_3 nanocubes. *Sens. Actuators B Chem.* **2019**, *290*, 59–67. [CrossRef]
50. Barbosa, M.S.; Suman, P.H.; Kim, J.J.; Tuller, H.L.; Orlandi, M.O. Investigation of electronic and chemical sensitization effects promoted by Pt and Pd nanoparticles on single-crystalline SnO nanobelt-based gas sensors. *Sens. Actuators B Chem.* **2019**, *301*, 127055. [CrossRef]
51. Gębicki, J.; Kloskowski, A.; Chrzanowski, W.; Stepnowski, P.; Namiesnik, J. Application of Ionic Liquids in Amperometric Gas Sensors. *Crit. Rev. Anal. Chem.* **2016**, *46*, 122–138. [CrossRef]
52. Paul, A.; Muthukumar, S.; Prasad, S. Room-temperature ionic liquids for electrochemical application with special focus on gas sensors. *J. Electrochem. Soc.* **2019**, *167*, 037511. [CrossRef]
53. Zevenbergen, M.A.G.; Wouters, D.; Dam, V.-A.T.; Brongersma, S.H.; Crego-Calama, M. Electrochemical Sensing of Ethylene Employing a Thin Ionic-Liquid Layer. *Anal. Chem.* **2011**, *83*, 6300–6307. [CrossRef] [PubMed]
54. Li, Y.; Xiao, A.-S.; Zou, B.; Zhang, H.-X.; Yan, K.-L.; Lin, Y. Advances of metal–organic frameworks for gas sensing. *Polyhedron* **2018**, *154*, 83–97. [CrossRef]
55. Kumar, P.; Deep, A.; Kim, K.-H. Metal organic frameworks for sensing applications. *TrAC—Trends Anal. Chem.* **2015**, *73*, 39–53. [CrossRef]
56. Hu, M.-L.; Razavi, S.A.A.; Piroozzadeh, M.; Morsali, A. Sensing organic analytes by metal–organic frameworks: A new way of considering the topic. *Inorg. Chem. Front.* **2020**, *7*, 1598–1632. [CrossRef]
57. Abideen, Z.U.; Kim, J.-H.; Lee, J.-H.; Kim, J.-Y.; Mirzaei, A.; Kim, H.W.; Kim, S.S. Electrospun Metal Oxide Composite Nanofibers Gas Sensors: A Review. *J. Korean Ceram. Soc.* **2017**, *54*, 366–379. [CrossRef]
58. Wang, C.; Wang, Y.; Yang, Z.; Hu, N. Review of recent progress on graphene-based composite gas sensors. *Ceram. Int.* **2021**, *47*, 16367–16384. [CrossRef]
59. Love, C.; Nazemi, H.; El-Masri, E.; Ambrose, K.; Freund, M.S.; Emadi, A. A Review on Advanced Sensing Materials for Agricultural Gas Sensors. *Sensors* **2021**, *21*, 3423. [CrossRef]
60. Mirzaei, A.; Leonardi, S.G.; Neri, G. Detection of hazardous volatile organic compounds (VOCs) by metal oxide nanostructures-based gas sensors: A review. *Ceram. Int.* **2016**, *42*, 15119–15141. [CrossRef]
61. Wang, J.; Shen, H.; Xia, Y.; Komarneni, S. Light-activated room-temperature gas sensors based on metal oxide nanostructures: A review on recent advances. *Ceram. Int.* **2021**, *47*, 7353–7368. [CrossRef]
62. Amiri, V.; Roshan, H.; Mirzaei, A.; Neri, G.; Ayesh, A.I. Nanostructured Metal Oxide-Based Acetone Gas Sensors: A Review. *Sensors* **2020**, *20*, 3096. [CrossRef] [PubMed]
63. Wang, C.; Yin, L.; Zhang, L.; Xiang, D.; Gao, R. Metal Oxide Gas Sensors: Sensitivity and Influencing Factors. *Sensors* **2010**, *10*, 2088–2106. [CrossRef]

64. Moseley, P.T. Progress in the development of semiconducting metal oxide gas sensors: A review. *Meas. Sci. Technol.* **2017**, *28*, 082001. [CrossRef]
65. Adhikari, B.; Majumdar, S. Polymers in sensor applications. *Prog. Polym. Sci.* **2004**, *29*, 699–766. [CrossRef]
66. Yaghi, O.M.; O'Keeffe, M.; Ockwig, N.W.; Chae, H.K.; Eddaoudi, M.; Kim, J. Reticular synthesis and the design of new materials. *Nature* **2003**, *423*, 705–714. [CrossRef]
67. Furukawa, H.; Cordova, K.E.; O'Keeffe, M.; Yaghi, O.M. The Chemistry and Applications of Metal-Organic Frameworks. *Science* **2013**, *341*, 1230444. [CrossRef] [PubMed]
68. Bo, R.; Taheri, M.; Liu, B.; Ricco, R.; Chen, H.; Amenitsch, H.; Fusco, Z.; Tsuzuki, T.; Yu, G.; Ameloot, R.; et al. Hierarchical Metal-Organic Framework Films with Controllable Meso/Macroporosity. *Adv. Sci.* **2020**, *7*, 2002368. [CrossRef]
69. Taheri, M.; Bernardo, I.D.; Lowe, A.; Nisbet, D.R.; Tsuzuki, T. Green Full Conversion of ZnO Nanopowders to Well-Dispersed Zeolitic Imidazolate Framework-8 (ZIF-8) Nanopowders via a Stoichiometric Mechanochemical Reaction for Fast Dye Adsorption. *Cryst. Growth Des.* **2020**, *20*, 2761–2773. [CrossRef]
70. Chen, D.; Zhao, J.; Zhang, P.; Dai, S. Mechanochemical synthesis of metal–organic frameworks. *Polyhedron* **2019**, *162*, 59–64. [CrossRef]
71. Schukraft, G.; Petit, C. Green Synthesis and Engineering Applications of Metal–Organic Frameworks. In *Sustainable Nanoscale Engineering*; Szekely, G., Livingston, A., Eds.; Elsevier: Amsterdam, The Netherlands, 2020; pp. 139–162.
72. Kumar, S.; Jain, S.; Nehra, M.; Dilbaghi, N.; Marrazza, G.; Kim, K.-H. Green synthesis of metal–organic frameworks: A state-of-the-art review of potential environmental and medical applications. *Coord. Chem. Rev.* **2020**, *420*, 213407. [CrossRef]
73. Zhao, Y.; Song, Z.; Li, X.; Sun, Q.; Cheng, N.; Lawes, S.; Sun, X. Metal organic frameworks for energy storage and conversion. *Energy Storage Mater.* **2016**, *2*, 35–62. [CrossRef]
74. Yang, J.; Yang, Y.W. Metal–Organic Frameworks for Biomedical Applications. *Small* **2020**, *16*, 1906846. [CrossRef] [PubMed]
75. Zhang, H.; Nai, J.; Yu, L.; Lou, X.W. Metal-Organic-Framework-Based Materials as Platforms for Renewable Energy and Environmental Applications. *Joule* **2017**, *1*, 77–107. [CrossRef]
76. Taheri, M.; Ashok, D.; Sen, T.; Enge, T.G.; Verma, N.K.; Tricoli, A.; Lowe, A.; Nisbet, D.R.; Tsuzuki, T. Stability of ZIF-8 nanopowders in bacterial culture media and its implication for antibacterial properties. *Chem. Eng. J.* **2021**, *413*, 127511. [CrossRef]
77. Liu, B.; Taheri, M.; Torres, J.F.; Fusco, Z.; Lu, T.; Liu, Y.; Tsuzuki, T.; Yu, G.; Tricoli, A. Janus Conductive/Insulating Microporous Ion-Sieving Membranes for Stable Li–S Batteries. *ACS Nano* **2020**, *14*, 13852–13864. [CrossRef]
78. Song, L.-F.; Jiang, C.-H.; Jiao, C.-L.; Zhang, J.; Sun, L.-X.; Xu, F.; You, W.-S.; Wang, Z.-G.; Zhao, J.-J. Two New Metal−Organic Frameworks with Mixed Ligands of Carboxylate and Bipyridine: Synthesis, Crystal Structure, and Sensing for Methanol. *Cryst. Growth Des.* **2010**, *10*, 5020–5023. [CrossRef]
79. Achmann, S.; Hagen, G.; Kita, J.; Malkowsky, I.; Kiener, C.; Moos, R. Metal-Organic Frameworks for Sensing Applications in the Gas Phase. *Sensors* **2009**, *9*, 1574–1589. [CrossRef]
80. Yao, M.-S.; Lv, X.-J.; Fu, Z.-H.; Li, W.-H.; Deng, W.-H.; Wu, G.-D.; Xu, G. Layer-by-Layer Assembled Conductive Metal-Organic Framework Nanofilms for Room-Temperature Chemiresistive Sensing. *Angew. Chem.* **2017**, *129*, 16737–16741. [CrossRef]
81. Arul, C.; Moulaee, K.; Donato, N.; Iannazzo, D.; Lavanya, N.; Neri, G.; Sekar, C. Temperature modulated Cu-MOF based gas sensor with dual selectivity to acetone and NO_2 at low operating temperatures. *Sens. Actuators B Chem.* **2021**, *329*. [CrossRef]
82. Koo, W.T.; Jang, J.S.; Kim, I.D. Metal-Organic Frameworks for Chemiresistive Sensors. *Chem* **2019**, *5*, 1938–1963. [CrossRef]
83. Lai, C.; Wang, Z.; Qin, L.; Fu, Y.; Li, B.; Zhang, M.; Liu, S.; Li, L.; Yi, H.; Liu, X.; et al. Metal-organic frameworks as burgeoning materials for the capture and sensing of indoor VOCs and radon gases. *Coord. Chem. Rev.* **2021**, *427*, 213565. [CrossRef]
84. Gamonal, A.; Sun, C.; Mariano, A.L.; Fernandez-Bartolome, E.; Guerrero-Sanvicente, E.; Vlaisavljevich, B.; Castells-Gil, J.; Marti-Gastaldo, C.; Poloni, R.; Wannemacher, R.; et al. Divergent Adsorption-Dependent Luminescence of Amino-Functionalized Lanthanide Metal–Organic Frameworks for Highly Sensitive NO_2 Sensors. *J. Phys. Chem. Lett.* **2020**, *11*, 3362–3368. [CrossRef] [PubMed]
85. Ma, Y.-X.; Gao, B.; Li, Y.; Wei, W.; Zhao, Y.; Ma, J.-F. Macrocycle-Based Metal–Organic Frameworks with NO_2-Driven On/Off Switch of Conductivity. *ACS Appl. Mater. Interfaces* **2021**, *13*, 27066–27073. [CrossRef]
86. Small, L.J.; Henkelis, S.E.; Rademacher, D.X.; Schindelholz, M.E.; Krumhansl, J.L.; Vogel, D.J.; Nenoff, T.M. Near-Zero Power MOF-Based Sensors for NO_2 Detection. *Adv. Funct. Mater.* **2020**, *30*, 2006598. [CrossRef]
87. Liu, Y.; Wang, R.; Zhang, T.; Liu, S.; Fei, T. Zeolitic imidazolate framework-8 (ZIF-8)-coated In_2O_3 nanofibers as an efficient sensing material for ppb-level NO_2 detection. *J. Colloid Interface Sci.* **2019**, *541*, 249–257. [CrossRef]
88. Jo, Y.-M.; Lim, K.; Yoon, J.W.; Jo, Y.K.; Moon, Y.K.; Jang, H.W.; Lee, J.-H. Visible-Light-Activated Type II Heterojunction in Cu_3(hexahydroxytriphenylene)$_2$/Fe_2O_3 Hybrids for Reversible NO_2 Sensing: Critical Role of π–π^* Transition. *ACS Cent. Sci.* **2021**, *7*, 1176–1182. [CrossRef]
89. Koo, W.T.; Kim, S.J.; Jang, J.S.; Kim, D.H.; Kim, I.D. Catalytic Metal Nanoparticles Embedded in Conductive Metal–Organic Frameworks for Chemiresistors: Highly Active and Conductive Porous Materials. *Adv. Sci.* **2019**, *6*, 1900250. [CrossRef] [PubMed]
90. Kim, J.-O.; Koo, W.-T.; Kim, H.; Park, C.; Lee, T.; Hutomo, C.A.; Choi, S.Q.; Kim, D.S.; Kim, I.-D.; Park, S. Large-area synthesis of nanoscopic catalyst-decorated conductive MOF film using microfluidic-based solution shearing. *Nat. Commun.* **2021**, *12*. [CrossRef]
91. Zhan, M.; Hussain, S.; AlGarni, T.S.; Shah, S.; Liu, J.; Zhang, X.; Ahmad, A.; Javed, M.S.; Qiao, G.; Liu, G. Facet controlled polyhedral ZIF-8 MOF nanostructures for excellent NO_2 gas-sensing applications. *Mater. Res. Bull.* **2021**, *136*, 111133. [CrossRef]

92. Zhang, J.; Liu, F.; Gan, J.; Cui, Y.; Li, B.; Yang, Y.; Qian, G. Metal-organic framework film for fluorescence turn-on H_2S gas sensing and anti-counterfeiting patterns. *Sci. China Mater.* **2019**, *62*, 1445–1453. [CrossRef]
93. Yassine, O.; Shekhah, O.; Assen, A.H.; Belmabkhout, Y.; Salama, K.N.; Eddaoudi, M. H_2S Sensors: Fumarate-Based fcu-MOF Thin Film Grown on a Capacitive Interdigitated Electrode. *Angew. Chem.* **2016**, *128*, 16111–16115. [CrossRef]
94. Wu, X.; Xiong, S.; Gong, Y.; Gong, Y.; Wu, W.; Mao, Z.; Liu, Q.; Hu, S.; Long, X. MOF-SMO hybrids as a H_2S sensor with superior sensitivity and selectivity. *Sens. Actuators B Chem.* **2019**, *292*, 32–39. [CrossRef]
95. Ali, A.; Alzamly, A.; Greish, Y.E.; Bakiro, M.; Nguyen, H.L.; Mahmoud, S.T. A Highly Sensitive and Flexible Metal–Organic Framework Polymer-Based H_2S Gas Sensor. *ACS Omega* **2021**, *6*, 17690–17697. [CrossRef]
96. Smith, M.K.; Mirica, K.A. Self-Organized Frameworks on Textiles (SOFT): Conductive Fabrics for Simultaneous Sensing, Capture, and Filtration of Gases. *J. Am. Chem. Soc.* **2017**, *139*, 16759–16767. [CrossRef]
97. Meng, Z.; Aykanat, A.; Mirica, K.A. Welding Metallophthalocyanines into Bimetallic Molecular Meshes for Ultrasensitive, Low-Power Chemiresistive Detection of Gases. *J. Am. Chem. Soc.* **2019**, *141*, 2046–2053. [CrossRef]
98. Wang, M.; Guo, L.; Cao, D. Amino-Functionalized Luminescent Metal–Organic Framework Test Paper for Rapid and Selective Sensing of SO_2 Gas and Its Derivatives by Luminescence Turn-On Effect. *Anal. Chem.* **2018**, *90*, 3608–3614. [CrossRef]
99. Zhang, J.; Xia, T.; Zhao, D.; Cui, Y.; Yang, Y.; Qian, G. In situ secondary growth of Eu(III)-organic framework film for fluorescence sensing of sulfur dioxide. *Sens. Actuators B Chem.* **2018**, *260*, 63–69. [CrossRef]
100. Chernikova, V.; Yassine, O.; Shekhah, O.; Eddaoudi, M.; Salama, K.N. Highly sensitive and selective SO_2 MOF sensor: The integration of MFM-300 MOF as a sensitive layer on a capacitive interdigitated electrode. *J. Mater. Chem. A* **2018**, *6*, 5550–5554. [CrossRef]
101. Dmello, M.E.; Sundaram, N.G.; Singh, A.; Singh, A.K.; Kalidindi, S.B. An amine functionalized zirconium metal–organic framework as an effective chemiresistive sensor for acidic gases. *Chem. Commun.* **2019**, *55*, 349–352. [CrossRef]
102. Ingle, N.; Sayyad, P.; Deshmukh, M.; Bodkhe, G.; Mahadik, M.; Al-Gahouari, T.; Shirsat, S.; Shirsat, M.D. A chemiresistive gas sensor for sensitive detection of SO_2 employing Ni-MOF modified –OH-SWNTs and –OH-MWNTs. *Appl. Phys. A* **2021**, *127*. [CrossRef]
103. Kim, K.-J.; Lu, P.; Culp, J.T.; Ohodnicki, P.R. Metal–Organic Framework Thin Film Coated Optical Fiber Sensors: A Novel Waveguide-Based Chemical Sensing Platform. *ACS Sens.* **2018**, *3*, 386–394. [CrossRef]
104. Stassen, I.; Dou, J.-H.; Hendon, C.; Dincă, M. Chemiresistive Sensing of Ambient CO_2 by an Autogenously Hydrated Cu_3(hexaiminobenzene)$_2$ Framework. *ACS Cent. Sci.* **2019**, *5*, 1425–1431. [CrossRef]
105. Dmello, M.E.; Sundaram, N.G.; Kalidindi, S.B. Assembly of ZIF-67 Metal-Organic Framework over Tin Oxide Nanoparticles for Synergistic Chemiresistive CO_2 Gas Sensing. *Chem. Eur. J.* **2018**, *24*, 9220–9223. [CrossRef] [PubMed]
106. Zhang, J.; Yue, D.; Xia, T.; Cui, Y.; Yang, Y.; Qian, G. A luminescent metal-organic framework film fabricated on porous Al_2O_3 substrate for sensitive detecting ammonia. *Microporous Mesoporous Mater.* **2017**, *253*, 146–150. [CrossRef]
107. Assen, A.H.; Yassine, O.; Shekhah, O.; Eddaoudi, M.; Salama, K.N. MOFs for the Sensitive Detection of Ammonia: Deployment of fcu-MOF Thin Films as Effective Chemical Capacitive Sensors. *ACS Sens.* **2017**, *2*, 1294–1301. [CrossRef] [PubMed]
108. Chen, X.; Lu, Y.; Dong, J.; Ma, L.; Yi, Z.; Wang, Y.; Wang, L.; Wang, S.; Zhao, Y.; Huang, J.; et al. Ultrafast In Situ Synthesis of Large-Area Conductive Metal–Organic Frameworks on Substrates for Flexible Chemiresistive Sensing. *ACS Appl. Mater. Interfaces* **2020**, *12*, 57235–57244. [CrossRef]
109. Campbell, M.G.; Sheberla, D.; Liu, S.F.; Swager, T.M.; Dincă, M. Cu_3(hexaiminotriphenylene)$_2$: An Electrically Conductive 2D Metal-Organic Framework for Chemiresistive Sensing. *Angew. Chem. Int. Ed.* **2015**, *54*, 4349–4352. [CrossRef] [PubMed]
110. Lin, Y.; Li, W.-H.; Wen, Y.; Wang, G.-E.; Ye, X.; Xu, G. Layer-by-layer Growth of Preferred-Oriented MOF Thin Film on Nanowire Array for High-Performance Chemiresistive Sensing. *Angew. Chem. Int. Ed.* **2021**. [CrossRef]
111. Khan, F.U.; Mehmood, S.; Zhao, X.; Yang, Y.; Pan, X. Ultra-Sensitive Bimetallic Alloy Loaded with Porous Architecture MOF for Ammonia Detection at Room Temperature. In Proceedings of the 2021 IEEE International Symposium on Circuits and Systems (ISCAS), Daegu, Korea, 22–28 May 2021.
112. Reddy, A.J.M.; Katari, N.K.; Nagaraju, P.; Surya, S.M. ZIF-8, Zn(NA) and Zn(INA) MOFs as chemical selective sensors of ammonia, formaldehyde and ethanol gases. *Mater. Chem. Phys.* **2020**, *241*, 122357. [CrossRef]
113. Li, Y.-P.; Li, S.-N.; Jiang, Y.-C.; Hu, M.-C.; Zhai, Q.-G. A semiconductor and fluorescence dual-mode room-temperature ammonia sensor achieved by decorating hydroquinone into a metal–organic framework. *Chem. Commun.* **2018**, *54*, 9789–9792. [CrossRef] [PubMed]
114. Travlou, N.A.; Singh, K.; Rodríguez-Castellón, E.; Bandosz, T.J. Cu–BTC MOF–graphene-based hybrid materials as low concentration ammonia sensors. *J. Mater. Chem. A* **2015**, *3*, 11417–11429. [CrossRef]
115. Gaba, A.; Felicia, S. Reduction of Air Pollution by Combustion Processes. In *The Impact of Air Pollution on Health, Economy, Environment and Agricultural Sources*; InTech: London, UK, 2011; pp. 119–142.
116. WHO. *Air Quality Guidelines for Particulate Matter, Ozone, Nitrogen Dioxide and Sulfur Dioxide: Global Update 2005*; WHO: Geneva, Switzerland, 2006.
117. Chen, T.-M.; Kuschner, W.G.; Gokhale, J.; Shofer, S. Outdoor Air Pollution: Nitrogen Dioxide, Sulfur Dioxide, and Carbon Monoxide Health Effects. *Am. J. Med. Sci.* **2007**, *333*, 249–256. [CrossRef]
118. Zhang, J.; Hu, E.; Liu, F.; Li, H.; Xia, T. Growth of robust metal–organic framework films by spontaneous oxidation of a metal substrate for NO_2 sensing. *Mater. Chem. Front.* **2021**. [CrossRef]

119. Moscoso, F.G.; Almeida, J.; Sousaraei, A.; Lopes-Costa, T.; Silva, A.M.G.; Cabanillas-Gonzalez, J.; Cunha-Silva, L.; Pedrosa, J.M. Luminescent MOF crystals embedded in PMMA/PDMS transparent films as effective NO_2 gas sensors. *Mol. Syst. Des. Eng.* **2020**, *5*, 1048–1056. [CrossRef]
120. Liu, C.; Kuang, Q.; Xie, Z.; Zheng, L. The effect of noble metal (Au, Pd and Pt) nanoparticles on the gas sensing performance of SnO_2-based sensors: A case study on the {221} high-index faceted SnO_2 octahedra. *CrystEngComm* **2015**, *17*, 6308–6313. [CrossRef]
121. Kolmakov, A.; Klenov, D.O.; Lilach, Y.; Stemmer, S.; Moskovits, M. Enhanced Gas Sensing by Individual SnO_2 Nanowires and Nanobelts Functionalized with Pd Catalyst Particles. *Nano Lett.* **2005**, *5*, 667–673. [CrossRef]
122. Majhi, S.M.; Naik, G.K.; Lee, H.-J.; Song, H.-G.; Lee, C.-R.; Lee, I.-H.; Yu, Y.-T. Au@NiO core-shell nanoparticles as a p-type gas sensor: Novel synthesis, characterization, and their gas sensing properties with sensing mechanism. *Sens. Actuators B Chem.* **2018**, *268*, 223–231. [CrossRef]
123. Lee, J.-C.; Kim, J.-O.; Lee, H.-J.; Shin, B.; Park, S. Meniscus-Guided Control of Supersaturation for the Crystallization of High Quality Metal Organic Framework Thin Films. *Chem. Mater.* **2019**, *31*, 7377–7385. [CrossRef]
124. Meng, C.; Cui, X.; Qi, S.; Zhang, J.; Kang, J.; Zhou, H. Lung inflation with hydrogen sulfide during the warm ischemia phase ameliorates injury in rat donor lungs via metabolic inhibition after cardiac death. *Surgery* **2017**, *161*, 1287–1298. [CrossRef]
125. Zhou, X.; Lin, X.; Yang, S.; Zhu, S.; Chen, X.; Dong, B.; Bai, X.; Wen, X.; Geyu, L.; Song, H. Highly dispersed Metal–Organic-Framework-Derived Pt nanoparticles on three-dimensional macroporous ZnO for trace-level H_2S sensing. *Sens. Actuators B Chem.* **2020**, *309*, 127802. [CrossRef]
126. Ding, M.; Cai, X.; Jiang, H.-L. Improving MOF stability: Approaches and applications. *Chem. Sci.* **2019**, *10*, 10209–10230. [CrossRef]
127. U.S. Environmental Protection Agency. Primary National Ambient Air Quality Standard for Sulfur Dioxide; Final Rule. *Fed. Regist.* **2010**, *75*, 35520–35603.
128. Zhou, Q.; Zeng, W.; Chen, W.; Xu, L.; Kumar, R.; Umar, A. High sensitive and low-concentration sulfur dioxide (SO_2) gas sensor application of heterostructure NiO-ZnO nanodisks. *Sens. Actuators B Chem.* **2019**, *298*, 126870. [CrossRef]
129. Liu, L.; Liu, S. Oxygen Vacancies as an Efficient Strategy for Promotion of Low Concentration SO_2 Gas Sensing: The Case of Au-Modified SnO_2. *ACS Sustain. Chem. Eng.* **2018**, *6*, 13427–13434. [CrossRef]
130. Wang, X.; Yao, F.; Xu, P.; Li, M.; Yu, H.; Li, X. Quantitative Structure–Activity Relationship of Nanowire Adsorption to SO_2 Revealed by In Situ TEM Technique. *Nano Lett.* **2021**, *21*, 1679–1687. [CrossRef] [PubMed]
131. Chaudhary, V.; Singh, H.; Kaur, A. Effect of charge carrier transport on sulfur dioxide monitoring performance of highly porous polyaniline nanofibres. *Polym. Int.* **2017**, *66*, 699–704. [CrossRef]
132. Zhao, C.H.; Gong, H.M.; Niu, G.Q.; Wang, F. Ultrasensitive SO_2 sensor for sub-ppm detection using Cu-doped SnO_2 nanosheet arrays directly grown on chip. *Sens. Actuators B Chem.* **2020**, *324*. [CrossRef]
133. Li, Q.; Wu, J.; Huang, L.; Gao, J.; Zhou, H.; Shi, Y.; Pan, Q.; Zhang, G.; Du, Y.; Liang, W. Sulfur dioxide gas-sensitive materials based on zeolitic imidazolate framework-derived carbon nanotubes. *J. Mater. Chem. A* **2018**, *6*, 12115–12124. [CrossRef]
134. Zhang, D.; Wu, D.; Zong, X.; Yang, Z. Enhanced SO_2 gas sensing properties of metal organic frameworks-derived titanium dioxide/reduced graphene oxide nanostructure. *J. Mater. Sci. Mater. Electron.* **2019**, *30*, 11070–11078. [CrossRef]
135. Su, P.-G.; Zheng, Y.-L. Room-temperature ppb-level SO_2 gas sensors based on RGO/WO_3 and MWCNTs/WO_3 nanocomposites. *Anal. Methods* **2021**, *13*, 782–788. [CrossRef] [PubMed]
136. Hoang, N.D.; Van Cat, V.; Nam, M.H.; Phan, V.N.; Le, A.T.; Van Quy, N. Enhanced SO_2 sensing characteristics of multi-wall carbon nanotubes based mass-type sensor using two-step purification process. *Sens. Actuators A Phys.* **2019**, *295*, 696–702. [CrossRef]
137. Tan, K.; Zuluaga, S.; Wang, H.; Canepa, P.; Soliman, K.; Cure, J.; Li, J.; Thonhauser, T.; Chabal, Y.J. Interaction of Acid Gases SO_2 and NO_2 with Coordinatively Unsaturated Metal Organic Frameworks: M-MOF-74 (M = Zn, Mg, Ni, Co). *Chem. Mater.* **2017**, *29*, 4227–4235. [CrossRef]
138. Hungerford, J.; Bhattacharyya, S.; Tumuluri, U.; Nair, S.; Wu, Z.; Walton, K.S. DMOF-1 as a Representative MOF for SO_2 Adsorption in Both Humid and Dry Conditions. *J. Phys. Chem. C* **2018**, *122*, 23493–23500. [CrossRef]
139. Savage, M.; Cheng, Y.; Easun, T.L.; Eyley, J.E.; Argent, S.P.; Warren, M.R.; Lewis, W.; Murray, C.; Tang, C.C.; Frogley, M.D.; et al. Selective Adsorption of Sulfur Dioxide in a Robust Metal–Organic Framework Material. *Adv. Mater.* **2016**, *28*, 8705–8711. [CrossRef] [PubMed]
140. Brandt, P.; Xing, S.-H.; Liang, J.; Kurt, G.; Nuhnen, A.; Weingart, O.; Janiak, C. Zirconium and Aluminum MOFs for Low-Pressure SO_2 Adsorption and Potential Separation: Elucidating the Effect of Small Pores and NH_2 Groups. *ACS Appl. Mater. Interfaces* **2021**, *13*, 29137–29149. [CrossRef] [PubMed]
141. Sapsanis, C.; Omran, H.; Chernikova, V.; Shekhah, O.; Belmabkhout, Y.; Buttner, U.; Eddaoudi, M.; Salama, K. Insights on Capacitive Interdigitated Electrodes Coated with MOF Thin Films: Humidity and VOCs Sensing as a Case Study. *Sensors* **2015**, *15*, 18153–18166. [CrossRef]
142. Seesaard, T.; Kerdcharoen, T.; Wongchoosuk, C. Hybrid materials with carbon nanotubes for gas sensing. In *Semiconductor Gas Sensors*, 2nd ed.; Jaaniso, R., Tan, O.K., Eds.; Woodhead Publishing: Sawston, UK, 2020; pp. 185–222.
143. Ma, P.-C.; Liu, M.-Y.; Zhang, H.; Wang, S.-Q.; Wang, R.; Wang, K.; Wong, Y.-K.; Tang, B.-Z.; Hong, S.-H.; Paik, K.-W.; et al. Enhanced Electrical Conductivity of Nanocomposites Containing Hybrid Fillers of Carbon Nanotubes and Carbon Black. *ACS Appl. Mater. Interfaces* **2009**, *1*, 1090–1096. [CrossRef]

144. Ingle, N.; Mane, S.; Sayyad, P.; Bodkhe, G.; Al-Gahouari, T.; Mahadik, M.; Shirsat, S.; Shirsat, M.D. Sulfur Dioxide (SO_2) Detection Using Composite of Nickel Benzene Carboxylic (Ni_3BTC_2) and OH-Functionalized Single Walled Carbon Nanotubes (OH-SWNTs). *Front. Mater. Sci.* **2020**, *7*, 93. [CrossRef]
145. Mao, S.; Lu, G.; Chen, J. Nanocarbon-based gas sensors: Progress and challenges. *J. Mater. Chem. A* **2014**, *2*, 5573. [CrossRef]
146. Boucher, O.; Friedlingstein, P.; Collins, B.; Shine, K.P. The indirect global warming potential and global temperature change potential due to methane oxidation. *Environ. Res. Lett.* **2009**, *4*, 044007. [CrossRef]
147. Hou, H.; Peng, S.; Xu, J.; Yang, S.; Mao, Z. Seasonal variations of CH_4 and N_2O emissions in response to water management of paddy fields located in Southeast China. *Chemosphere* **2012**, *89*, 884–892. [CrossRef] [PubMed]
148. Ritchie, H.; Roser, M. CO_2 and Greenhouse Gas Emission. Available online: https://ourworldindata.org/co2-and-other-greenhouse-gas-emissions (accessed on 22 August 2021).
149. Ramalho, O.; Wyart, G.; Mandin, C.; Blondeau, P.; Cabanes, P.-A.; Leclerc, N.; Mullot, J.-U.; Boulanger, G.; Redaelli, M. Association of carbon dioxide with indoor air pollutants and exceedance of health guideline values. *Build Environ.* **2015**, *93*, 115–124. [CrossRef]
150. Jacobson, T.A.; Kler, J.S.; Hernke, M.T.; Braun, R.K.; Meyer, K.C.; Funk, W.E. Direct human health risks of increased atmospheric carbon dioxide. *Nat. Sustain.* **2019**, *2*, 691–701. [CrossRef]
151. Talin, A.A.; Centrone, A.; Ford, A.C.; Foster, M.E.; Stavila, V.; Haney, P.; Kinney, R.A.; Szalai, V.; El Gabaly, F.; Yoon, H.P.; et al. Tunable Electrical Conductivity in Metal-Organic Framework Thin-Film Devices. *Science* **2014**, *343*, 66–69. [CrossRef]
152. Strauss, I.; Mundstock, A.; Treger, M.; Lange, K.; Hwang, S.; Chmelik, C.; Rusch, P.; Bigall, N.C.; Pichler, T.; Shiozawa, H.; et al. Metal–Organic Framework Co-MOF-74-Based Host–Guest Composites for Resistive Gas Sensing. *ACS Appl. Mater. Interfaces* **2019**, *11*, 14175–14181. [CrossRef] [PubMed]
153. García, E.J.; Mowat, J.P.S.; Wright, P.A.; Pérez-Pellitero, J.; Jallut, C.; Pirngruber, G.D. Role of Structure and Chemistry in Controlling Separations of CO_2/CH_4 and $CO_2/CH_4/CO$ Mixtures over Honeycomb MOFs with Coordinatively Unsaturated Metal Sites. *J. Phys. Chem. C* **2012**, *116*, 26636–26648. [CrossRef]
154. Chen, Z.; Deng, S.; Wei, H.; Wang, B.; Huang, J.; Yu, G. Activated carbons and amine-modified materials for carbon dioxide capture—A review. *Front. Environ. Sci. Eng.* **2013**, *7*, 326–340. [CrossRef]
155. Davey, A.K.; Gao, X.; Xia, Y.; Li, Z.; Dods, M.N.; Delacruz, S.; Pan, A.; Swamy, S.; Gardner, D.; Carraro, C.; et al. Amine-functionalized metal-organic framework ZIF-8 toward colorimetric CO_2 sensing in indoor air environment. *Sens. Actuators B Chem.* **2021**, *344*, 130313. [CrossRef]
156. Yoon, B.; Choi, S.-J.; Swager, T.M.; Walsh, G.F. Switchable Single-Walled Carbon Nanotube–Polymer Composites for CO_2 Sensing. *ACS Appl. Mater. Interfaces* **2018**, *10*, 33373–33379. [CrossRef]
157. Srinives, S.; Sarkar, T.; Hernandez, R.; Mulchandani, A. A miniature chemiresistor sensor for carbon dioxide. *Anal. Chim. Acta* **2015**, *874*, 54–58. [CrossRef]
158. Liu, G.K.; Zhu, L.J.; Yu, Y.M.; Qiu, M.; Gao, H.J.; Chen, D.Y. WO_3 nanoplates for sensitive and selective detections of both acetone and NH_3 gases at different operating temperatures. *J. Alloys Compd.* **2021**, *858*. [CrossRef]
159. Saidi, T.; Zaim, O.; Moufid, M.; El Bari, N.; Ionescu, R.; Bouchikhi, B. Exhaled breath analysis using electronic nose and gas chromatography–mass spectrometry for non-invasive diagnosis of chronic kidney disease, diabetes mellitus and healthy subjects. *Sens. Actuators B Chem.* **2018**, *257*, 178–188. [CrossRef]
160. Mitrayana, M.; Ma'arif, M.A.; Wasono, M.A.J.; Satriawan, M.; Ikhsan, M.R. Application of the CO_2 laser photoacoustic spectroscopy in detecting ammonia gas (NH_3) in liver disease patients breath. *Key Eng. Mater.* **2020**, *840*, 399–405. [CrossRef]
161. Hwang, K.; Ahn, J.; Cho, I.; Kang, K.; Kim, K.; Choi, J.; Polychronopoulou, K.; Park, I. Microporous Elastomer Filter Coated with Metal Organic Frameworks for Improved Selectivity and Stability of Metal Oxide Gas Sensors. *ACS Appl. Mater. Interfaces* **2020**, *12*, 13338–13347. [CrossRef] [PubMed]
162. Yao, M.S.; Xiu, J.W.; Huang, Q.Q.; Li, W.H.; Wu, W.W.; Wu, A.Q.; Cao, L.A.; Deng, W.H.; Wang, G.E.; Xu, G. Van der Waals Heterostructured MOF-on-MOF Thin Films: Cascading Functionality to Realize Advanced Chemiresistive Sensing. *Angew. Chem.* **2019**, *131*, 15057–15061. [CrossRef]